

On the Anisotropic Gaussian Velocity Closure for Inertial-Particle Laden Flows

Aymeric Vié^{1,2,5,*}, François Doisneau^{1,2,3} and Marc Massot^{1,2,4,‡}

¹ CNRS Laboratoire EM2C - UPR 288, Grande Voie des Vignes, 92295 Chatenay-Malabry, France.

² Ecole Centrale Paris, Grande Voie des Vignes, 92295 Chatenay-Malabry, France.

³ ONERA, Chemin de la Hunière, 91120, Palaiseau France.

⁴ Fédération de Mathématiques de l'Ecole Centrale Paris, FR CNRS 3487, France.

⁵ Center For Turbulence Research, Stanford University, 488, Escondido Mall, Stanford CA 94305-3035, USA.

Received 2 December 2013; Accepted (in revised version) 14 May 2014

Abstract. The accurate simulation of disperse two-phase flows, where a discrete particulate condensed phase is transported by a carrier gas, is crucial for many applications; Eulerian approaches are well suited for high performance computations of such flows. However when the particles from the disperse phase have a significant inertia compared to the time scales of the flow, particle trajectory crossing (PTC) occurs i.e. the particle velocity distribution at a given location can become multi-valued. To properly account for such a phenomenon many Eulerian moment methods have been recently proposed in the literature. The resulting models hardly comply with a full set of desired criteria involving: 1- ability to reproduce the physics of PTC, at least for a given range of particle inertia, 2- well-posedness of the resulting set of PDEs on the chosen moments as well as guaranteed realizability, 3- capability of the model to be associated with a high order realizable numerical scheme for the accurate resolution of particle segregation in turbulent flows. The purpose of the present contribution is to introduce a multi-variate Anisotropic Gaussian closure for such particulate flows, in the spirit of the closure that has been suggested for out-of-equilibrium gas dynamics and which satisfies the three criteria. The novelty of the contribution is three-fold. First we derive the related moment system of conservation laws with source terms, and justify the use of such a model in the context of high Knudsen numbers, where collision operators play no role. We exhibit the main features and advantages in terms of mathematical structure and realizability. Then a second order accurate and realizable MUSCL/HLL scheme is proposed and validated. Finally the behavior of the method for the description of PTC is thoroughly investigated and its ability to account accurately for inertial particulate flow dynamics in typical configurations is assessed.

*Corresponding author. *Email addresses:* aymeric.vie@stanford.edu, aymeric.vie@ecp.fr (A. Vié), francois.doisneau@ecp.fr (F. Doisneau), marc.massot@ecp.fr (M. Massot)

†Presently at CTR, Stanford University, formerly postdoctoral fellow at EM2C Laboratory (2011-2013).

‡Visiting Professor at Stanford University, CTR (2011-2012).

AMS subject classifications: 76T10, 76P05, 82C21, 65M08, 35L40, 52B55

Key words: Particulate flows, kinetic theory, moment method, particle trajectory crossing.

1 Motivation and objective

Two-phase flows constituted of a gaseous phase carrying a disperse condensed phase play a key role in many industrial and scientific applications e.g. spray combustion in Diesel engines or aeronautical combustors, soot dynamics, fluidized beds. In all these applications the disperse phase is composed of particles/droplets of various sizes that can possibly coalesce or aggregate, break-up, evaporate and have their own inertia and size-conditioned dynamics.

To describe the disperse phase, many strategies can be envisioned. In the present work, we consider the dynamics of the particulate phase in a statistical sense using a kinetic approach and we describe it using a Number Density Function (NDF). The NDF measures an ensemble average (over a given set of initial conditions) number of particles at a specific location in the phase space. The phase space is determined by the number of internal coordinates that describe the particle state: position, velocity, size, temperature, *etc.*. These variables evolve due to physical phenomena: transport, drag force, evaporation, heating, *etc.* which are accounted for through a Williams-Boltzmann Equation (WBE) [76], also called a Generalized Population Balance Equation (GPBE) in other scientific communities (chemical engineering, aerosol science).

There are several strategies to solve this kinetic equation: a direct resolution in the full phase space through deterministic methods is too expensive and beyond reach in most practical cases. A second choice is to approximate the NDF by a sample of discrete numerical parcels describing particles of various internal coordinates through a Lagrangian-Monte-Carlo approach [1, 25, 37, 56]. It is called Direct Simulation Monte-Carlo method (DSMC) in [8] and is generally considered to be the most accurate method for solving this type of WBE; it is specially suited for direct numerical simulations (DNS) on canonical configurations since it does not introduce any numerical diffusion. However, the number of parcels required to achieve a satisfactory statistical convergence comes to be high in 3D cases, especially when a high number of internal coordinates is required, and such an approach is no longer suitable for practical applications.

To overcome this limitation, Macroscopic Eulerian Moment Methods offer a promising alternative. Instead of solving the NDF itself, the WBE is integrated over selected dimensions of the phase space, including in particular velocity [19, 40]. Moment equations are obtained with a new phase space of reduced dimension, for which deterministic methods of discretization are affordable and efficient. The coordinate of the phase space which is the most essential to deal with is the velocity, because it will drive the spatial distribution of particles. Thus in the following we will focus on distributions which are monodisperse in all variables except velocity. Additional dimensions of the phase space

can still be accounted for, such as the size phase space, and we refer to Appendix A for a general methodology and references. Even with this non-restrictive level of simplification, the main drawback of such methods is that some level of information is lost while integrating over the velocity phase space, that is when describing the disperse phase through a limited number of well-chosen velocity moments. Consequently designing an accurate moment method mainly relies on a physics-dependent choice for the moment structure and on its link with the underlying NDF and WBE.

In the present work we are interested in the description of the dynamics of inertial particles in a gaseous carrier phase. In such flows the motion of particles strongly depends on their inertia characterized by their Stokes number, i.e. the ratio between their relaxation time and a characteristic time scale of the carrier phase. For instance in turbulent flows the Kolmogorov time scale of the gas can be considered. For Stokes numbers below one the particulate phase velocity is strongly correlated to the gas phase velocity and previous studies have shown that Eulerian methods are able to capture properly the physics [3]: The velocity distribution is properly approximated by a hydrodynamic equilibrium assumption called a Monokinetic velocity distribution*, thus involving only a small set of low order moments. Several methods exist for this range of Stokes numbers [28, 42, 48] that are widely used in the literature (see for example [20] and references therein). But when the Stokes number is above one, the velocity distribution is no longer Monokinetic because of the occurrence of Particle Trajectory Crossing (PTC) referred to as the Random Uncorrelated Motion in [29], and more moments are needed to describe it. We divide up the approaches of the literature into two categories:

- Algebraic-Closure-Based Moment Methods (ACBMM): A limited set of moments, usually up to the second order moments, are chosen and transported. Since their transport involves higher order moments, these missing moments are computed from the knowledge of the lower order moments through “equilibrium assumptions” inspired from RANS turbulence modeling using explicit algebraic closures [65]. One example of this class of methods introduced in [50, 51] considers and transports a unique, scalar second order moment. Other second or third order moments are then computed from the knowledge of the transported moments to get the most accurate closure at a reduced cost. This type of approach has already reached the real application level [49, 60, 63, 72]. However it has to face local realizability problems [64], i.e. the occurrence of moments linked to a non-positive NDF, and the design of adapted numerics is not straightforward and has never been conducted since the mathematical structure of the underlying system of PDEs is not clearly identified.
- Kinetic-Based Moment Methods (KBMM): The main idea of this type of approach is to consider a set of moments for which we can associate in a one-to-one correspondence a unique kinetic velocity distribution with a sufficient number of parameters

*A Maxwell-Boltzmann distribution at zero temperature, that is all the particles have the same velocity at a given position and time.

to control the given set of moments. This presumed NDF must be positive and allows to evaluate high order moments needed in the system of PDEs for transport. Closures have been proposed to control moments up to the first order (Monokinetic closure [42]), up to the second order [53], up to the third order (CQMOM [78]), and up to the fourth order (Multi Gaussian [43]). Among the KBMM two categories emerge; the first is based on hydrodynamic equilibrium usually related to a given notional collision operator and the second is based on quadrature methods. The first category allows a well-defined mathematical structure and entropy inequality, whereas most of the time the second leads to weakly hyperbolic systems [16]. The main advantage with KBMM is the existence of dedicated numerical methods, which will guarantee the realizability and the stable behavior of the numerical schemes, either classical hyperbolic solvers [44,68] or kinetic schemes [11,19,78].

In the present work, KBMM of the first category are preferred because of their inherent advantages over ACBMM in terms of realizability, mathematical structure and numerical scheme design. We propose a method that can control moments up to the second order: the Anisotropic Gaussian closure (AG). This closure has already been introduced in the context of out-of-equilibrium rarefied gases [46], and is chosen for several reasons:

- The first evidence of PTC is a non-zero velocity variance, described by internal “agitation” energy, which needs at least second order moments to be captured;
- Such a closure has good mathematical properties for rarefied gases [2,36] at both kinetic and moment levels;
- The resulting system of partial differential equations is proven to be hyperbolic and admits entropies.

The main interest in using this closure rather than more complex ones such as CQMOM or Multi-Gaussian, beyond the advantages in terms of mathematical structure and entropy inequality for the treatment of singularities, is a matter of cost: we seek the best compromise in terms of number of moments versus reproduction of the physics of the particulate flow. Second order moments may be in fact sufficient to capture such physics in a large range of Stokes number, as long as such methods are able to connect to the zone where the velocity distribution is Monokinetic i.e. where macroscopic internal energy is zero.

The scope of the present contribution is three-fold. First we derive the related moment system of conservation laws with source terms, we justify the use of such a model in the context of high Knudsen numbers (which are classical in a large range of particulate flows where collision operators play no role), and we exhibit the main features and advantages in terms of mathematical structure and realizability. The potential of an Eulerian method cannot be fairly assessed without then considering the related numerical strategy [19]: we therefore develop a new dedicated numerical scheme, that is robust and realizable. We design a second order accurate and realizable MUSCL/HLL scheme; it is presented

and validated. Finally the behavior of the method for the description of PTC is then thoroughly investigated, and its ability to account accurately for inertial particulate flow dynamics in typical configurations relevant to the real applications is assessed.

The paper is organized in the following way. In Section 2 we introduce the AG model for a disperse phase with a discussion about the justification of such an approach for disperse phase flows and the resulting moment equations. In Section 3 we describe a new second order MUSCL-HLL scheme, based on a realizable reconstruction of the primitive variables. In Section 4 the numerical methods are evaluated on 1D cases and an emphasis is made on the necessity of a proper handling of vacuum zones. In Section 5, the level of description of the AG model is assessed on a 2D crossing jet configuration that mimics the simplest crossing that can occur. In Section 6 the new approach is assessed on model turbulent flows. Results on 2D Taylor-Green vortices and a 2D decaying turbulence are compared to a Lagrangian reference and to a so-called Isotropic Gaussian closure to assess the significance of anisotropy for such flows. In the prospect of realistic applications the extension to 3D structured and unstructured meshes is discussed in the conclusion.

2 The 10-moment Anisotropic Gaussian (AG) velocity closure

2.1 Kinetic description of a disperse phase

In the present work we consider dilute particulate flows under the point-particle approximation. Therefore the disperse phase is completely described at a mesoscopic level [30,52] by its Number Density Function (NDF) $f(t, \mathbf{x}, \mathbf{u})$, where $f d\mathbf{x}d\mathbf{u}$ denotes the average number of droplets (in a statistical sense), at time t , in a volume of size $d\mathbf{x}$ around a space location \mathbf{x} , with a velocity in a $d\mathbf{u}$ -neighborhood of \mathbf{u} .

The evolution of the NDF is described by a Boltzmann-like equation, the Williams transport equation [76,77]. Considering a simplified model where only local momentum exchange with the gas due to drag force and convective fluxes are described, as well as particles interactions, it reads:

$$\partial_t f + \mathbf{c} \cdot \partial_{\mathbf{x}} f + \partial_{\mathbf{c}} \cdot (\mathbf{F}f) = \Gamma(f), \quad (2.1)$$

where \mathbf{F} is the drag acceleration per unit mass and $\Gamma(f)$ the collision/coalescence operator describing the particle/particle interactions. These terms require models that should take into account physical phenomena at the particle scale. As an illustration the Stokes law can model \mathbf{F} when the particular Reynolds number is moderate. This acceleration per unit mass is due to the velocity difference with the gaseous phase:

$$\mathbf{F}(t, \mathbf{x}, \mathbf{c}) = \frac{\mathbf{u}_g(t, \mathbf{x}) - \mathbf{c}}{\tau_p}, \quad \tau_p = \frac{\rho_l d_p^2}{18\mu_g}, \quad (2.2)$$

where $\mathbf{u}_g(t, \mathbf{x})$ is the gas velocity, μ_g its dynamic viscosity, d_p the particle diameter and ρ_l

its material density[†]. The details of the modeling of $\Gamma(f)$ will not be provided since this operator will be discarded in the following; however details can be found in [21].

Since a direct resolution of Eq. (2.1) through deterministic methods would not be efficient given the dimension of the phase space, we envision a resolution of some moments of the NDF:

$$M_{i,j,k}(t, \mathbf{x}) = \iiint c_1^i c_2^j c_3^k f(t, \mathbf{x}, \mathbf{c}) d\mathbf{c} = \langle c_1^i c_2^j c_3^k f \rangle. \quad (2.3)$$

Eq. (2.1) is integrated over the phase space and conservation equations on moments are obtained:

$$\partial_t M_{i,j,k} + \partial_{\mathbf{x}} \cdot \begin{pmatrix} M_{i+1,j,k} \\ M_{i,j+1,k} \\ M_{i,j,k+1} \end{pmatrix} = -\frac{1}{\tau_p} \left[(i+j+k) M_{i,j,k} - \mathbf{u}_{\mathbf{g}} \cdot \begin{pmatrix} i M_{i-1,j,k} \\ j M_{i,j-1,k} \\ k M_{i,j,k-1} \end{pmatrix} \right]. \quad (2.4)$$

This system of conservation laws lives in a 3D space that can be efficiently discretized and solved for instance in a finite volume framework. The resolution will require the evaluation of fluxes and will rely on the mathematical structure of the system associated with the closure solution: for every moment set of order N containing all moments for which $i+j+k \leq N$, moments of order $N+1$ are required to describe the fluxes in the physical space. The moment method we choose will then consist in determining (1) the moment set that is solved, (2) the closure that enables to find the unknown fluxes, and (3) the mathematical structure and potential entropy inequalities in order to identify the nature of solutions and design a numerical scheme.

2.2 Kinetic-based moment methods of second order and its relation to rarefied gas dynamics

Before detailing the requirements on our closure and the associated kinetic description, we first introduce some definitions:

- A moment vector \mathcal{M} of order N is realizable if there exist a non-negative NDF, the moments of which up to order N are exactly the components of \mathcal{M} . By extension a NDF is denoted realizable if it is non-negative.
- The moment space is the set of moment vectors that are realizable. The moment space is a convex space[‡].

For number density functions, the support of which is defined on a compact set in 1D, the finite moment problem, called the Hausdorff moment problem, has an infinite

[†]Let us underline that we focus on simple models for the sake of legibility of the paper but the present analysis can be extended to both more complex models [19,27] and to two-way coupled configurations [21]; however, the evaluation of the model will be conducted in a much more systematic way in the present setting, without interfering with model additional difficulties.

[‡]In the usual gas dynamics framework it is also denoted the set of admissible states and is an open convex set [31].

number of solutions for moment vectors inside the moment space, whereas a unique solution can be found by the maximization of entropy in the sense of Shannon (see [54] and references therein), with potential difficulties in the neighborhood of the frontier of the moment space. Similarly, in our case, where the velocity phase space is \mathbb{R}^d , namely the multidimensional Hamburger moment problem [70], we would like to rely on a one-to-one correspondence between the moment vector and an underlying NDF through a similar entropy formalism. One way to do it is to use the hydrodynamic limit such as for the normal solutions of the Boltzmann equation, which lead to Euler fluid equations for the moment vector [4, 32, 45]. However such an approach usually relies on the structure of collision operators, whereas we deal with an infinite Knudsen number framework. Let us first recall some results from kinetic theory and then envision what we can learn for particulate flows.

2.2.1 Kinetic theory for rarefied gases

In the context of kinetic theory and rarefied gases, this Hamburger problem has been largely investigated. Actually in such flows the kinetic equation is the following:

$$\partial_t f + \mathbf{c} \cdot \partial_{\mathbf{x}} f = \mathcal{C}(f), \quad (2.5)$$

where $\mathcal{C}(f)$ is the Boltzmann collision operator. This collision operator has several properties [32, 34]:

- Mass $\langle f \rangle$, momentum $\langle \mathbf{c}f \rangle$, and energy $\langle \mathbf{c}^2 f \rangle$ are invariant through collisions.
- $\mathcal{C}(f)$ satisfies a local dissipation of the entropy $\mathcal{H}(f) = \langle f \ln f \rangle$, i.e. $\langle \mathcal{C}(f) \ln(f) \rangle < 0$. Eq. (2.5) has consequently an associated \mathcal{H} -theorem.
- The local equilibrium is the Maxwell-Boltzmann distribution:

$$f_{eq}(t, \mathbf{x}, \mathbf{c}) = \frac{\rho}{(2\pi)^{\frac{3}{2}} \sqrt{\Theta}} \exp\left(-\frac{(\mathbf{c} - \mathbf{u})^2}{2\Theta}\right), \quad (2.6)$$

where $\rho = \langle f \rangle$, $\mathbf{u} = \langle \mathbf{c}f \rangle$ and $\Theta = \langle (\mathbf{u} - \mathbf{c})^2 f \rangle$.

For small Knudsen number the NDF can be sought as an expansion about this Maxwell-Boltzmann equilibrium distribution and zero and first order expansions generate the classical Euler and Navier-Stokes systems of equations respectively, for which total density, momentum, and energy equations have to be solved. As for the Navier-Stokes equations, such a perturbative approach can lead to realizability problems [47].

To approximate the collision operator for such types of flows, simplified operators have been proposed in the literature. The most famous one is the BGK operator [7]:

$$\mathcal{C}(f) = \frac{f_{eq} - f}{\tau_c}, \quad (2.7)$$

where τ_c is the collision time. The kernel of this operator is the equilibrium Maxwell-Boltzmann distribution. Then for small Knudsen numbers, the classical Euler system of equations can be obtained. For higher Knudsen numbers, this collision operator leads to the Navier-Stokes system of equations. However it always predicts a Prandtl number of unity, whereas typical Prandtl numbers for gases are actually less than unity. To correct the BGK model Holway [36] proposed a modified version of the BGK operator: instead of using the Maxwell-Boltzmann distribution as the kernel of the collision operator, he uses a linear combination, parameterized by ν , of the Maxwell-Boltzmann distribution and an Anisotropic Gaussian distribution that has the same moments as the NDF up to second order, sometimes referred to as the ellipsoidal distribution leading to the so-called ES-BGK collision operator [13, 67]:

$$f_{ME}^{\nu}(\mathbf{c}) = \frac{\rho}{(2\pi)^{\frac{3}{2}} |\boldsymbol{\Sigma}_{\nu}|^{\frac{1}{2}}} \exp\left(-\frac{1}{2}(\mathbf{c}-\mathbf{u})^T \boldsymbol{\Sigma}_{\nu}^{-1}(\mathbf{c}-\mathbf{u})\right), \quad (2.8)$$

where $\boldsymbol{\Sigma}_{\nu} = \nu \boldsymbol{\Theta} + (1-\nu) \frac{1}{3}(\text{tr} \boldsymbol{\Theta}) \mathbf{I}$, with $\boldsymbol{\Theta} = \frac{1}{\rho} \langle [(\mathbf{c}-\mathbf{u}) \otimes (\mathbf{c}-\mathbf{u})] f \rangle$. The AG distribution has been chosen based on the maximization of the Shannon entropy (the opposite of the microscopic Entropy $\mathcal{H}(f)$): among the infinite number of possible distributions which fulfill the moment constraints and rotational invariance, only this family maximizes the Shannon entropy for a given range of ν [36]. Such distributions can be viewed as the most probable distribution given the knowledge on the moments. This combination is parameterized in such a way that the Prandtl number can be modified through ν and the behavior of classical gases can be reproduced [36, 67]. The proposed extended BGK operator, for the proper range of ν , has been proven to fulfill the \mathcal{H} -theorem in [2].

For higher Knudsen numbers when larger non-equilibrium effects have to be taken into account, relying on perturbative methods and expansions around an equilibrium distribution may not be accurate. Several methods exist in the literature to account for more complexity for this type of flows. Grad [33] has developed high order closures, such as the Grad-13 theory. However these methods encounter realizability issues, as they are based on a NDF that cannot be guaranteed non-negative. In this context, this AG distribution has been later placed in a hierarchy of modeling approaches by Levermore and Morokoff [45], where the authors suggested to use NDFs based on Entropy maximization using larger and larger sets of moments, thus being more and more accurate. As mentioned by Levermore and Morokoff [46], this distribution provides an intermediate level of description between Euler and Navier Stokes equations, without relying on expansions. Higher order closures based on entropy maximization have also been considered; in [14, 43, 55] the authors analyze both the model and the numerics, especially in terms of realizability. However the inversion of highly non-linear systems, along with higher order methods, becomes cumbersome for practical applications.

The main interest of closures avoiding a perturbation method is that:

- (1) They are intrinsically realizable as they rely on non-negative NDFs;

- (2) They fulfill entropy dissipation conditions that are mandatory to respect a \mathcal{H} -theorem on the microscopic entropy, which is the basis of a physically sound system and provides entropy inequalities at the macroscopic level;
- (3) They always yield hyperbolic systems of equations at the moment level [45].

2.2.2 Particle-laden flows

Back to the WBE Eq. (2.1) for the description of particulate flows, collisions, even if present through the term $\Gamma(f)$, are considered as negligible since the dilute regime leads to very large Knudsen numbers. Thus we cannot expect a relaxation towards an equilibrium distribution corresponding to hydrodynamic limit such as in the collisional flows encountered in gas dynamics. However the drag acceleration plays the role of a dissipation phenomenon and can be shown, in the presence of Brownian motion or subgrid turbulent agitation, to lead to Maxwell-Boltzmann equilibrium distribution in the limit of a zero Stokes number [17,80]. In this context we know that for sufficiently small Stokes numbers, the assumption of a hydrodynamic limit at zero temperature is valid as long as PTC does not take place [19,52] and it leads to pressureless gas dynamics equations. For slightly larger Stokes numbers, we expect that second order moment methods following the line presented previously should be able to capture properly PTC and connect naturally with pressureless gas dynamics.

Let us underline that PTC, in this context is going to be treated statistically, in the sense that it will not be deterministically resolved such as in CQMOM or Multi-Gaussian higher order moment methods, but its impact will be described through an energy of agitation. The last ingredient we need is related to the fact the PTC can be highly anisotropic and such an energy has to be directional and cannot be described by an isotropic model (see in particular Section 5). Inspired by the work of [45,46], we consider the Anisotropic Gaussian model.

It is important at this level to insist on the fact that we do not only close the system of PDEs on the moments up to second order by assuming that the central moments of order three are zero. The present model comes with an entropy formalism through the correspondence between the moment level and the kinetic distribution and enables to treat singularities naturally appearing in moment conservation equations. Besides, hyperbolicity provides a warrant that such singularities can be controlled.

Hereafter, we justify such a choice using several arguments:

- Entropy Maximization: the AG distribution is the most probable velocity distribution, with the constraint that the second order moments are fixed, following the Maximization of Shannon entropy [36], and is also the minimum of microscopic entropy [2]. We will thus make an assumption of local hydrodynamic equilibrium.
- Hyperbolicity: a great interest compared to ACBMM or Grad-13 theory is that the generated moment system is hyperbolic, making it a good candidate to Godunov-type solvers, which can cope with singularity formation.

- Entropic structure: the macroscopic system of equations we will consider is in fact the limit for zero Knudsen numbers of the following equation:

$$\partial_t \tilde{f} + \mathbf{c} \cdot \partial_{\mathbf{x}} \tilde{f} + \partial_{\mathbf{c}} \cdot (\mathbf{F} \tilde{f}) = \Gamma(\tilde{f}) + \mathcal{C}_r(\tilde{f}), \quad (2.9)$$

which is an approximation of (2.5), where we rely on an additional “notional” collision operator:

$$\mathcal{C}_r(\tilde{f}) = \frac{\tilde{f}_{ME}^v - \tilde{f}}{\tau_r}, \quad (2.10)$$

with the constraint that \tilde{f}_{ME}^v has the same moments up to order two as \tilde{f} and the notional collisional time τ_r is taken in the zero limit. Let us underline that there is a fundamental difference between the case $\nu \in [-1/2, 0) \cup (0, 1]$ and the case $\nu = 0$, which we are going to consider. In the former range, studied in [2], the collisional invariants are the usual collisional invariant of the Boltzmann operator that is only the trace of the energy covariance matrix is involved, whereas in the latter, the full covariance matrix becomes a collisional invariant. In the sequel, we will consider the case $\nu = 0$ since we want to minimize the impact in the moment equation of the notional collision operator. Eq. (2.9) admits a \mathcal{H} -theorem, as well as an entropy inequality at macroscopic level. Besides the macroscopic contribution of the original and physical collision operator $\Gamma(f)$ can be evaluated (we will dismiss that in the following) as in [46]. The resulting system of macroscopic conservation equations is thus obtained through Maxwell transfer equations, using the form of the equilibrium AG distribution obtained in the $\tau_r \rightarrow 0$ limit.

2.3 The Anisotropic Gaussian moment system

In this subsection the resulting system of conservation laws with source terms is derived from the kinetic description using the previously introduced ingredients. We consider a 2D physical space, but all the proposed developments can be extended to 3D space in a straightforward manner.

2.3.1 System of conservation laws with source terms

First, we define the macroscopic quantities of interest, which are the zero, first and second order central moments:

$$\rho = M_{0,0}, \quad u = \frac{M_{1,0}}{M_{0,0}}, \quad v = \frac{M_{0,1}}{M_{0,0}}, \quad (2.11a)$$

$$\sigma_{11} = \frac{M_{2,0}}{M_{0,0}} - u^2, \quad \sigma_{12} = \frac{M_{1,1}}{M_{0,0}} - uv, \quad \sigma_{22} = \frac{M_{0,2}}{M_{0,0}} - v^2, \quad (2.11b)$$

where ρ is total number density, u and v the mean velocities in x and y directions, and σ_{11} , σ_{12} and σ_{22} the covariances in x , $x-y$ and y directions. Taking the Maxwell transfer equation Eq. (2.9) in the limit of zero τ_r at hydrodynamic equilibrium leads after integration

over the velocity phase space to the following system of conservation laws with source terms related to the drag acceleration:

$$\partial_t \mathcal{M} + \partial_x \cdot \mathcal{F}(\mathcal{M}) = \mathcal{S}(\mathcal{M}), \quad (2.12)$$

where the moments \mathcal{M} and the fluxes $\mathcal{F} = (\mathcal{F}_x, \mathcal{F}_y)^T$ take the expression:

$$\mathcal{M} = \rho \begin{pmatrix} 1 \\ u \\ v \\ u^2 + \sigma_{11} \\ uv + \sigma_{12} \\ v^2 + \sigma_{22} \end{pmatrix}, \quad \mathcal{F}_x = \rho \begin{pmatrix} u \\ u^2 + \sigma_{11} \\ uv + \sigma_{12} \\ u^3 + 3u\sigma_{11} \\ u^2v + 2u\sigma_{12} + v\sigma_{11} \\ uv^2 + u\sigma_{22} + 2v\sigma_{12} \end{pmatrix}, \quad (2.13a)$$

$$\mathcal{S} = \frac{\rho}{\tau_p} \begin{pmatrix} 0 \\ u_g - u \\ v_g - v \\ 2(uu_g - u^2 - \sigma_{11}) \\ uv_g + vu_g - 2uv - \sigma_{12} \\ 2(vv_g - v^2 - \sigma_{22}) \end{pmatrix}, \quad (2.13b)$$

and \mathcal{F}_y is deduced by obvious substitutions. We also define $\mathbf{P} = \rho \Sigma$ with

$$\Sigma = \begin{pmatrix} \sigma_{11} & \sigma_{12} \\ \sigma_{12} & \sigma_{22} \end{pmatrix}.$$

\mathcal{S} represents the relaxation of the particle velocities towards the one of the gas phase through drag force. In the limit of small τ_p , this term needs a specific numerical attention to recover the asymptotic tracer-like limit, for which the particles have the same velocity as the gas phase. In the present contribution we will focus on relaxation times that do not require a specific treatment in order to preserve accuracy, that is inertial particles. The reader may refer to [17] for details about how to capture the right asymptotic limit in the framework of Asymptotic-Preserving schemes.

2.3.2 Eigenstructure, hyperbolicity and entropies

The introduced formalism allows directly deducing the eigenvalues as well as hyperbolicity and entropies. The presentation of the present subsection is inspired from [6] and we restrict to a 1D configuration for the sake of clarity. Some subtleties of the multidimensional formulation will be studied as part of our next studies and will be essential for unstructured mesh simulation, but can be avoided in the Cartesian meshes we use in this paper. The system (2.12) is hyperbolic and admits the set of eigenvalues [6]:

$$\lambda_x = (u, u, u + \sqrt{\sigma_{11}}, u - \sqrt{\sigma_{11}}, u + \sqrt{3\sigma_{11}}, u - \sqrt{3\sigma_{11}})^T. \quad (2.14)$$

The eigenvalue u has two orders of multiplicity and is associated to a linearly degenerated field. The other eigenvalues have one order of multiplicity. The eigenvalues $u \pm \sqrt{3\sigma_{11}}$ are associated to genuinely nonlinear fields and the eigenvalues $u \pm \sqrt{\sigma_{11}}$ are associated to linearly degenerate fields.

The system (2.12) is also associated with two entropy families. We define the functions s_{11} and s_{12} :

$$s_{11} = \frac{p_{11}}{\rho^3} = \frac{\sigma_{11}}{\rho^2}, \quad s_{12} = \frac{p_{11}p_{22} - p_{12}^2}{\rho^4} = \frac{\sigma_{11}\sigma_{22} - \sigma_{12}^2}{\rho^2}. \quad (2.15)$$

A family of convex functions $\mathcal{F}(s_{11})$ and $\mathcal{G}(s_{12})$ resulting from the composition of the logarithm function and a functional that has some identified properties [6], as well as entropy fluxes $u\mathcal{F}(s_{11})$ and $u\mathcal{G}(s_{12})$ yield Lax entropy pairs of the system (2.12) and satisfy:

$$\partial_t \rho \mathcal{F}(s_{11}) + \partial_x (u \mathcal{F}(s_{11})) \leq 0, \quad \partial_t \rho \mathcal{G}(s_{12}) + \partial_x (u \mathcal{G}(s_{12})) \leq 0. \quad (2.16)$$

Such an approach allows treating the shocks that can naturally appear in Eulerian moment models and also to rely on the large literature devoted to Godunov-like schemes.

3 A realizable MUSCL/HLL scheme

In the Eulerian simulation of disperse phase flows, the choice of the numerics plays a significant role. Actually, the density field may encounter large variations, featuring at worst vacuum zones and stiff accumulations. Such singularities are difficult to capture and require high order adapted numerics. In the literature, many strategies can be found. Here is a non-exhaustive list of possible strategies:

- High order numerics with artificial viscosity: in the AVBP code the Eulerian moment equations are solved using a central scheme [18]. Due to their oscillatory behavior in the neighborhood of high gradients, the scheme is stabilized using artificial viscosity [23] that is user-defined. Such schemes can lead to accurate solutions [23] but need a non-negligible effort to find the most accurate set-up, while maintaining the stability of the computation.
- Second order kinetic schemes with slope limitations: to avoid numerous user-defined parameters, limited schemes are a classical alternative. For instance a second order kinetic scheme is used in [19] for the resolution of the Monokinetic Eulerian moment method [42]. Based on the work of [11], this scheme uses a limited linear and conservative reconstruction of density and velocities. For the linear reconstructed conservative values, the scheme offers an exact in time integration of fluxes at cell interfaces (the so-called non-local approach [10]) by making use of the underlying kinetic equation. Other works have used this type of scheme for more complex systems of equations [39].

- Second order MUSCL schemes [69]: depending on the moment system, an exact-in-time kinetic integration of the convective fluxes cannot always be used. To circumvent this issue, MUSCL schemes make use of a second order space reconstruction, a first order flux evaluation at cell interfaces, and a second order Runge-Kutta time integration. This type of scheme has for instance been proposed for Eulerian simulations in [74] and is also used in industrial oriented codes such as the CEDRE code at ONERA (see [20,58] and references therein).
- Relaxation schemes can also be used such as in [6,9] and see references therein. The key issue here is to design a second order in time and space that associates several criteria, such as realizability as well as proper asymptotic behavior in the limit of zero pressure as treated in [9] in the case of Euler equations. Thus, even if this is a promising path, we do not have all the ingredients at hand in order to build the final solver for the case we want to tackle.

As we require a robust and realizable method, high order schemes with artificial viscosity are not retained. Moreover, because of the complexity of the moment system, kinetic schemes are more difficult to handle and do not lead to accurate solutions. Finally, kinetic schemes are more difficult to handle in the framework of unstructured meshes and relaxation solvers still require some amount of work in order to comply with the program we have in mind for particle-laden flows. Thus we focus on the development of a second order MUSCL scheme.

In this work, a splitting strategy is used: the convection part and source part are treated separately using an Alternate Lie splitting, which is second order in time [44]. The convective part is also solved using a dimensional splitting. The splitting is used because it is easier to develop solvers that are proven to be realizable for each element of the full equation.

Then, we derive a second order MUSCL-HLL scheme with conservative reconstruction of primitive variables $\mathcal{U} = (\rho, u, v, \sigma_{11}, \sigma_{12}, \sigma_{22})^T$. This method is composed of two main steps:

1. Reconstruction: each variable is reconstructed within each cell to calculate interface values;
2. Flux evaluation: the fluxes are evaluated using the interface values with a first order flux. Using a RK2 method for the time integration, it provides a second order scheme in space and time.

In the present work we propose a reconstruction of the primitive variables ρ , u , and Σ because realizability conditions such as positivity of the energy are easier to impose on primitive variables. We also impose that our reconstruction is conservative i.e. the integral over the cells of the inner reconstruction is equal to the cell value, such as for kinetic schemes in [11], which is not classical in the framework of MUSCL scheme [6].

Hereafter we first detail the reconstruction strategy, the slope evaluation strategy being detailed in Appendix B. Then, the flux evaluation and the time integration are presented.

3.1 Conservativity and corrected cell values

To achieve a second order in space scheme, linear reconstructions are envisioned. A previous work from Berthon [5] has been devoted to the evaluation of several reconstruction strategies in the perspective of MUSCL schemes for Euler equations. In the present work, we propose a new reconstruction based on central moments, which has the advantage of being conservative and realizability-preserving. We consider a finite volume discretization over the x dimension into cells of characteristic size Δx . The reconstructed variables for the cell j are the density, the mean velocities and the covariance matrix (cell-reconstructed variables are noted $\tilde{\cdot}$):

$$\tilde{\mathcal{U}}_j(x) = \bar{\mathcal{U}}_j + \mathcal{D}\mathcal{U}(x - x_j), \quad (3.1)$$

where $\bar{\mathcal{U}}_j = (\rho_j, \bar{u}_j, \bar{v}_j, \bar{\sigma}_{11,j}, \bar{\sigma}_{12,j}, \bar{\sigma}_{22,j})^T$ and $\mathcal{D}\mathcal{U} = (D_{\rho_j}, D_{u_j}, D_{v_j}, D_{\sigma_{11,j}}, D_{\sigma_{12,j}}, D_{\sigma_{22,j}})^T$.

Classically, this type of reconstruction is done without a conservativity constraint [5], because it is just needed to evaluate the fluxes at the interface. But as our aim is to ensure the realizability of the moments through their time evolution, a conservative reconstruction guarantees that the fluxes will preserve realizability. Conservativity imposes to consider a corrected cell value for each reconstructed variable noted $\bar{\cdot}$. The subsequent constraints are the following:

$$M_{kl,j} = \frac{1}{\Delta x} \int_{x_{j-1/2}}^{x_{j+1/2}} \tilde{M}_{kl,j}(x) dx, \quad (3.2)$$

where $\tilde{M}_{kl,j}(x)$ is the reconstructed 2D velocity moment of order $k+l$ and $M_{kl,j}$ its mean values in the cell j . Then, for each moment, we get:

$$M_{00,j} = \rho_j, \quad M_{10,j} = \rho_j \bar{u}_j + D_{\rho_j} D_{u_j} \frac{\Delta x^2}{12}, \quad M_{01,j} = \rho_j \bar{v}_j + D_{\rho_j} D_{v_j} \frac{\Delta x^2}{12}, \quad (3.3a)$$

$$M_{20,j} = \rho_j (\bar{u}_j^2 + \bar{\sigma}_{11,j}) + \left(\rho_j D_{u_j}^2 + D_{\rho_j} (2\bar{u}_j D_{u_j} + D_{\sigma_{11,j}}) \right) \frac{\Delta x^2}{12}, \quad (3.3b)$$

$$M_{11,j} = \rho_j (\bar{u}_j \bar{v}_j + \bar{\sigma}_{12,j}) + \left(\rho_j D_{u_j} D_{v_j} + D_{\rho_j} (\bar{u}_j D_{u_j} + \bar{v}_j D_{v_j} + D_{\sigma_{12,j}}) \right) \frac{\Delta x^2}{12}, \quad (3.3c)$$

$$M_{02,j} = \rho_j (\bar{v}_j^2 + \bar{\sigma}_{22,j}) + \left(\rho_j D_{v_j}^2 + D_{\rho_j} (2\bar{v}_j D_{v_j} + D_{\sigma_{22,j}}) \right) \frac{\Delta x^2}{12}. \quad (3.3d)$$

The corrected cell values are then:

$$\bar{\rho}_j = \rho_j, \quad \bar{u}_j = u_j - \frac{D_{\rho_j} D_{u_j}}{\rho_j} \frac{\Delta x^2}{12}, \quad \bar{v}_j = v_j - \frac{D_{\rho_j} D_{v_j}}{\rho_j} \frac{\Delta x^2}{12}, \quad (3.4)$$

$$\bar{\Sigma}_j = \Sigma_j - \frac{\Delta x^2}{12} \alpha \mathbf{D}_{\mathbf{u}}^2 - \frac{\Delta x^2}{12} \frac{D_{\rho_j}}{\rho_j} \mathbf{D}_{\Sigma}, \quad (3.5)$$

where

$$\mathbf{D}^2_{\mathbf{u}} = \begin{pmatrix} D_{u_j}^2 & D_{u_j}D_{v_j} \\ D_{u_j}D_{v_j} & D_{v_j}^2 \end{pmatrix}, \quad \mathbf{D}_{\Sigma} = \begin{pmatrix} D_{\sigma_{11}} & D_{\sigma_{12}} \\ D_{\sigma_{12}} & D_{\sigma_{22}} \end{pmatrix}, \quad \alpha = 1 + \frac{\Delta x^2}{12} \frac{D_{\rho_j}^2}{\rho_j^2}.$$

To finish the reconstruction a slope evaluation strategy is required, which is detailed in Appendix B. The slope evaluation is complex because the slopes can lead to unrealizable corrected cell values. Moreover whereas the positivity of the central moments can be easily ensured, the positivity of the covariance matrix determinant imposes a non-linear constraint. Our slope evaluation satisfies the positivity of the density, the diagonal components of Σ , as well as its determinant. This limitation also imposes a maximum principle on each variable to avoid the generation of spurious oscillations.

3.2 Fluxes and time integration

Once the reconstruction strategy is provided, one has to decide how to solve the generalized Riemann problem (GRP) at each cell interface [68]. A classical strategy is to use a MUSCL scheme [69]: instead of solving the GRP, it solves a classical Riemann problem for which each state is defined as the right and left states at the interface position, given by the reconstruction strategy. Such a Riemann problem can be solved using first order Approximate Riemann solvers. This strategy has been extensively studied in [5] for the Euler equations using several reconstruction strategies. In the following we will use the same method: we will use the reconstruction strategy to evaluate the states at the interfaces and, for the purpose of proving the realizability preservation, we will consider a piecewise constant reconstruction in each cell. Then we will solve the Riemann problem at each interface using a first order HLL scheme [35] and finally embed it into a second order in time SSP-Runge Kutta scheme. The realizability of the scheme is proven if:

1. Using the linear reconstruction of the primitive variables to evaluate a piecewise constant reconstruction leads to realizable states;
2. The HLL scheme preserves the realizability;
3. The chosen Runge Kutta scheme preserves the realizability.

Let us introduce some notations. For a given reconstruction strategy, which is assumed to satisfy a realizability condition, we will associate a spatial reconstruction in the cell constituted of three constant states (M_L, M_C, M_R) , where M_L denotes the left boundary reconstructed state $M_L = \tilde{M}_j(x_j - \Delta x/2)$ and M_R denotes the right boundary reconstructed state $M_R = \tilde{M}_j(x_j + \Delta x/2)$. We want this new spatial reconstruction to be equivalent to the reconstruction previously introduced in the integral sense and further assume the width of the support of M_L is $\alpha_1 \Delta x$, $\alpha_1 \in [0, 1/2]$, the one of M_L is α_1 and the one of M_C is $1 - 2\alpha_1$. At this level we have to provide both α_1 and the middle state M_C . The following Theorem provides a way to evaluate these quantities.

Theorem 3.1. *Let us consider a linear reconstruction strategy in the j^{th} cell, which satisfies the realizability of the state vector at the cell interfaces. This reconstruction is equivalent in the integral sense to a realizable three constant substate spatial reconstruction (M_L, M_C, M_R) with respective supports $(x_j - \Delta x/2, x_j - \Delta x/2 + \alpha_1 \Delta x)$, $(x_j - \Delta x/2 + \alpha_1 \Delta x, x_j - \Delta x/2 + (1 - \alpha_1) \Delta x)$, $(x_j - \Delta x/2 + (1 - \alpha_1) \Delta x, x_j + \Delta x/2)$ and with $M_L = \tilde{M}_j(x_j - \Delta x/2)$ and $M_R = \tilde{M}_j(x_j + \Delta x/2)$, under the conditions $\alpha_1 = 1/6$ and*

$$\bar{\sigma}_{11}\bar{\sigma}_{22} - \bar{\sigma}_{12}^2 + \frac{\Delta x^4}{48} \frac{D_\rho^2}{\rho^2} (\bar{\sigma}_{11}D_v^2 + \bar{\sigma}_{22}D_u^2 - 2\bar{\sigma}_{12}D_uD_v) > 0.$$

The proof is provided in Appendix C. A consequence of the realizability conditions is that the CFL-like condition, which avoids interactions among Riemann problems at the various interfaces becomes:

$$\frac{\Delta t}{\Delta x} \max(\lambda) < \frac{1}{2} \min(\alpha_1, 1 - 2\alpha_1). \quad (3.6)$$

The realizability of the piecewise constant approximation being proven, we then apply a first order HLL scheme at each cell interface. Considering the moment equations for the advection in one direction:

$$\partial_t \mathcal{M} + \partial_x \mathcal{F}(\mathcal{M}) = 0. \quad (3.7)$$

Integrating Eq. (3.7) over x -direction across one cell interface $j+1/2$, one gets the intermediate state:

$$\mathcal{M}_{j+1/2}^* = \frac{\lambda_{\min}^j \mathcal{M}_j - \lambda_{\max}^{j+1} \mathcal{M}_{j+1}}{\lambda_{\min}^j - \lambda_{\max}^{j+1}} - \frac{\mathcal{F}(\mathcal{M}_j) - \mathcal{F}(\mathcal{M}_{j+1})}{\lambda_{\min}^j - \lambda_{\max}^{j+1}}, \quad (3.8)$$

where λ_{\min}^j and λ_{\max}^{j+1} are respectively the slowest and the fastest characteristic waves of the states in cells j and $j+1$. The fluxes are then computed at the interface:

$$\begin{aligned} \mathcal{F}_{j+1/2}^{HLL}(\mathcal{M}_j, \mathcal{M}_{j+1}) &= \frac{1}{2} (\mathcal{F}(\mathcal{M}_j) + \mathcal{F}(\mathcal{M}_{j+1})) \\ &\quad - \frac{1}{2} |\lambda_{\min}^j| (\mathcal{M}_{j+1/2}^* - \mathcal{M}_j) - \frac{1}{2} |\lambda_{\max}^{j+1}| (\mathcal{M}_{j+1} - \mathcal{M}_{j+1/2}^*). \end{aligned} \quad (3.9)$$

Theorem 3.2. *Let us assume that, $\forall j \in \mathbb{Z}$, M_j^n at time t^n is realizable. Under the condition $\lambda_{\min}^j < u_j - \sqrt{\sigma_{11,j}}$ and $\lambda_{\max}^j > u_j + \sqrt{\sigma_{11,j}}$, $\forall j \in \mathbb{Z}$, the intermediate states $\mathcal{M}_{j+1/2}^*$ at each cell interface are realizable. Under the CFL condition (3.6), the HLL scheme is realizable.*

The proof is also given in Appendix C. Finally the integration in time is performed using a two-step Runge-Kutta method. Two RK2 methods can be envisioned. The first one is the most used in applied simulations because it is the less memory-consuming:

$$\mathcal{M}_j^{n+1/2} = \mathcal{M}_j^n - \frac{1}{2} \frac{\Delta t}{\Delta x} \left(\mathcal{F}_{j+1/2}^{HLL}(\mathcal{M}_j^n, \mathcal{M}_{j+1}^n) - \mathcal{F}_{j-1/2}^{HLL}(\mathcal{M}_{j-1}^n, \mathcal{M}_j^n) \right), \quad (3.10a)$$

$$\mathcal{M}_j^{n+1} = \mathcal{M}_j^{n+1/2} - \frac{\Delta t}{\Delta x} \left(\mathcal{F}_{j+1/2}^{HLL}(\mathcal{M}_j^{n+1/2}, \mathcal{M}_{j+1}^{n+1/2}) - \mathcal{F}_{j-1/2}^{HLL}(\mathcal{M}_{j-1}^{n+1/2}, \mathcal{M}_j^{n+1/2}) \right). \quad (3.10b)$$

For such a scheme, realizability is hard to prove, whereas there exists another RK2 scheme for which realizability is demonstrated, as long as the basis first order scheme and the reconstruction are realizable:

$$\tilde{\mathcal{M}}_j = \mathcal{M}_j^n - \frac{\Delta t}{\Delta x} \left(\mathcal{F}_{j+1/2}^{HLL}(\mathcal{M}_j^n, \mathcal{M}_{j+1}^n) - \mathcal{F}_{j-1/2}^{HLL}(\mathcal{M}_{j-1}^n, \mathcal{M}_j^n) \right), \quad (3.11a)$$

$$\tilde{\tilde{\mathcal{M}}}_j = \tilde{\mathcal{M}}_j^n - \frac{\Delta t}{\Delta x} \left(\mathcal{F}_{j+1/2}^{HLL}(\tilde{\mathcal{M}}_j^n, \tilde{\mathcal{M}}_{j+1}^n) - \mathcal{F}_{j-1/2}^{HLL}(\tilde{\mathcal{M}}_{j-1}^n, \tilde{\mathcal{M}}_j^n) \right), \quad (3.11b)$$

$$\mathcal{M}_j^{n+1} = \frac{1}{2} \mathcal{M}_j^n + \frac{1}{2} \tilde{\tilde{\mathcal{M}}}_j. \quad (3.11c)$$

As it is a convex combination of states resulting from the first order scheme, this scheme is realizable. In the following, both schemes have been tested. Results shown here were obtained using the second RK2 scheme, whereas the other RK2 scheme leads to essentially the same results.

4 1D cases and vacuum treatment

We now evaluate both the modeling approach and the numerics. They are first studied on canonical test cases, which are expected to exhibit the accuracy, robustness and stability of the present method. Three cases are investigated:

- An initial value problem with transported smooth fields: this case is used to evaluate the order of accuracy of the numerical scheme;
- A Sod tube problem: this case from [6] is a standard test case to exhibit the ability of the scheme to reproduce the classical waves inherent to the 10-moment Anisotropic Gaussian model;
- A Sod tube problem with vacuum: interfaces with vacuum can generate high velocities and energies, that are highly constraining for explicit solvers. A regularization strategy is proposed that treats the problem with a controlled and limited effect on the accuracy.

4.1 Initial value problem with smooth transported fields

The smooth test case is designed to assess the order of accuracy of the newly introduced scheme, especially in comparison to the first order HLL scheme. The initial condition is a Gaussian profile in the x -direction $\rho = 1 + \exp\left(-\frac{(x-0.5)^2}{0.1^2}\right)$ with constant velocities $u = v = 1$ and constant pressures $p_{11} = p_{22} = 1.0$ and $p_{12} = 0.5$. The computation is done for $t = 1s$ at $CFL = 1/12$. Results of L^2 error on density are plotted in Fig. 1 and demonstrate the improvement of the MUSCL/HLL scheme compared to a classical HLL scheme. In particular, its order of precision is twice the one of the HLL scheme (respectively 1.6 and 0.79). Moreover, for moderate mesh refinements (200 cells), the second order scheme is

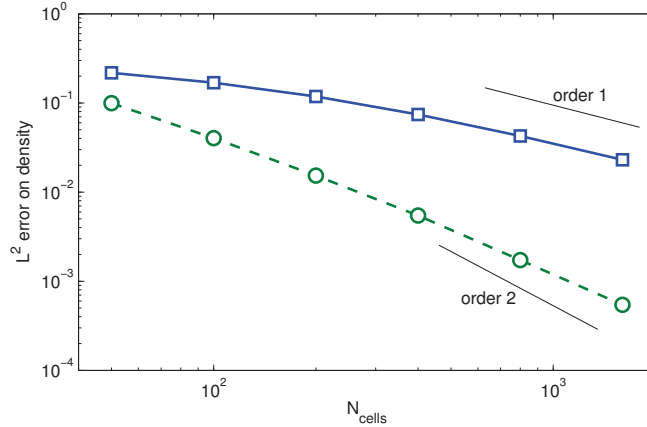


Figure 1: Smooth case: L^2 error versus the number of points for HLL (blue squares) and MUSCL/HLL (green circles) schemes.

one order of magnitude more accurate than the first order scheme, which will be helpful for the 2D cases investigated in this work, as well as for real 3D multi-scale problems.

4.2 Sod tube

The Sod tube is a classical problem to investigate the robustness and accuracy of Riemann solvers for hyperbolic problems. Here we have chosen to reproduce the test case proposed in [6] in order to show the impact of second order schemes on the treatment of singularities naturally arising in particle-laden flows. The initial conditions are summarized in Table 1. In Fig. 2 the HLL scheme and the new realizable MUSCL/HLL scheme, both at $\text{CFL} = 1/12$, are compared to a reference solution at time $t = 0.1$ s for which mesh convergence has been verified. Results show that the new MUSCL/HLL scheme obtains better results than the classical HLL scheme, reducing the smearing of every wave in the domain. The stability and the robustness of the method are also demonstrated, as no stabilization procedure is required.

Table 1: Initial conditions for the Sod tube problem.

	ρ	u	v	P_{11}	P_{12}	P_{22}
left state	1	0	0	2	0.05	0.6
right state	0.125	0	0	0.2	0.1	0.2

4.3 Treatment of interfaces with vacuum zones

The last test case is of primary importance for injection configurations, or any highly segregative conditions, which are met in two-phase flows. It is the same test case as for the

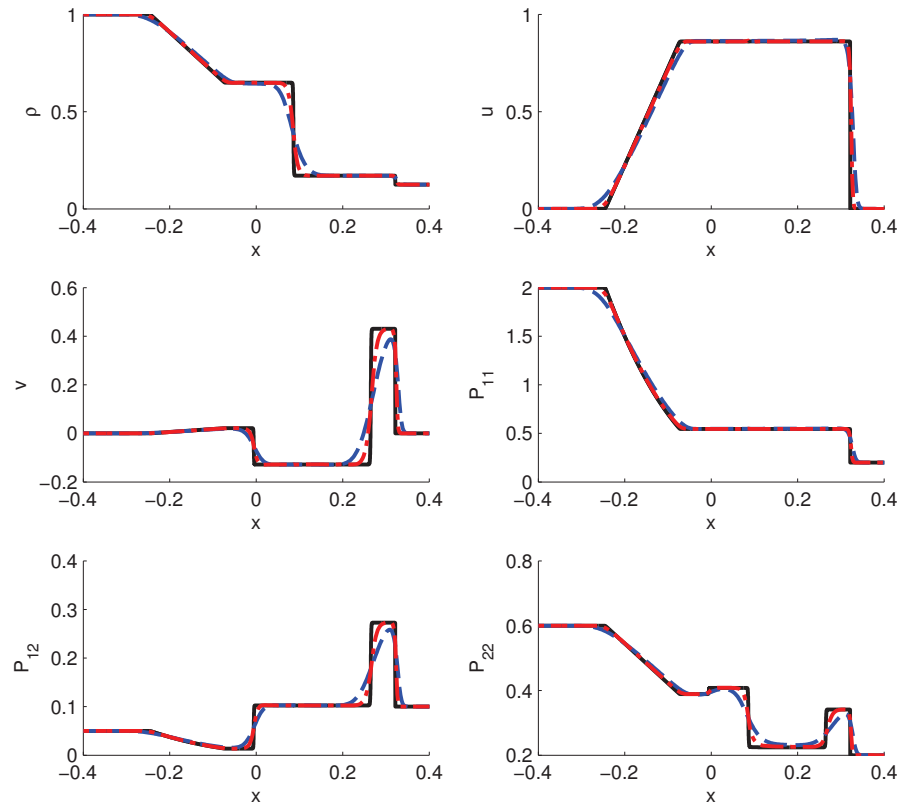


Figure 2: Sod tube problem at time $t=0.1$ s: reference solution (black line), HLL scheme (blue dashed line), and MUSCL/HLL scheme (red dot-dashed line) with 400 cells.

Sod tube problem but the right state has been replaced by vacuum, see Table 2. Similarly as for Euler equations the treatment of vacuum or low density zones may require some attention. For example Einfeldt et al. [26] have demonstrated that a Riemann solver based on a linearization cannot guarantee the positivity of the energy near low density zones, where Godunov-type schemes such as the HLL scheme can.

Table 2: Initial conditions for the Sod tube problem with vacuum.

	ρ	u	v	P_{11}	P_{12}	P_{22}
left state	1	0	0	2	0.05	0.6
right state	0.0	0	0	0.0	0.0	0.0

In Fig. 3 results obtained with HLL and MUSCL/HLL scheme are compared. At the interface with vacuum central moments such as velocity and internal energy are significant. Such singularities do not appear in density-weighted quantities, such as momentum and pressure. Actually the most divergent quantity is s_{11} , which reaches values of the order of 10^{20} . This entropy production is due to the HLL scheme approximation, so that

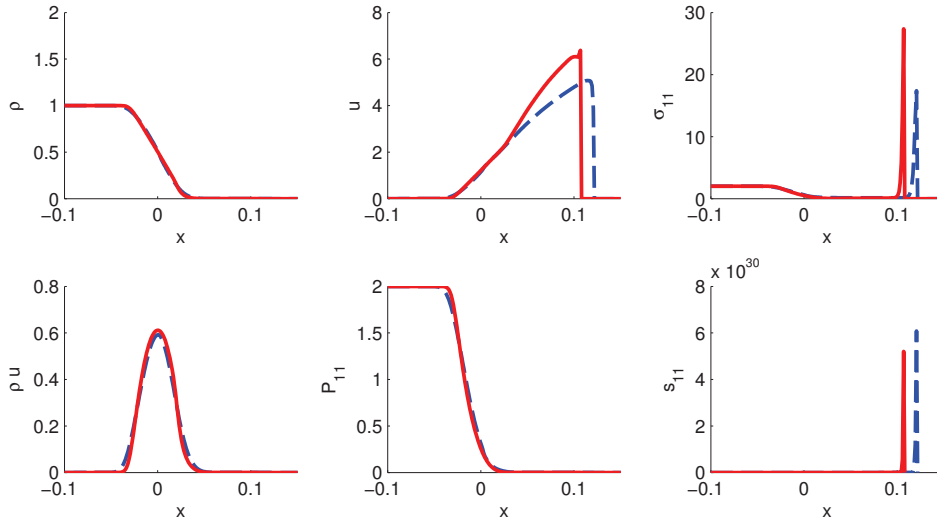


Figure 3: Riemann problem with vacuum at time $t=0.05$ s: HLL scheme (blue dashed line), and MUSCL/HLL scheme (red full line) with 200 cells.

it is purely due to the numerical scheme and not to the physics of the problem. To handle such a highly constraining behavior, the time step in explicit methods will be drastically reduced: a regularization procedure is suggested based on a limitation of the entropy in the system. This limitation will reduce this artificial generation of entropy, avoiding abnormally high internal energies and velocities. The procedure is the following:

$$\sigma_{corr} = \sigma \min(\alpha), \quad (4.1)$$

where:

$$\alpha_i = \begin{cases} 1 & \text{if } s_{ii} < S_{lim}; \\ S_{lim} + (S_{max} - S_{lim}) \tanh\left(\frac{s_{ii} - S_{lim}}{S_{max} - S_{lim}}\right) & \text{else,} \end{cases} \quad \text{for } i=1,2. \quad (4.2)$$

where S_{max} is the maximum entropy threshold and S_{lim} an entropy at which the limitation starts to act progressively up to S_{max} . In the case of entropies that are greater than the threshold S_{max} , all components of the internal energy are reduced in order to keep the same eigenvalues for the internal energy tensor. This limitation is expected to have a minor impact on the moment vector, as it acts in low density zones. The choice of the threshold is physics-dependent: as the internal energy is expected to reproduce crossings, a good estimate for this threshold is found to be related to events that generate crossings. For example, in a gas flow field, a good primary estimate is given by the variance of the gas velocity field and the mean number density in injection or droplets initial clouds.

In Fig. 4 results for the MUSCL/HLL scheme with and without limitations are shown. Two thresholds are tested: $S_{max} = 100$ and $S_{max} = 300$, which are respectively the maxi-

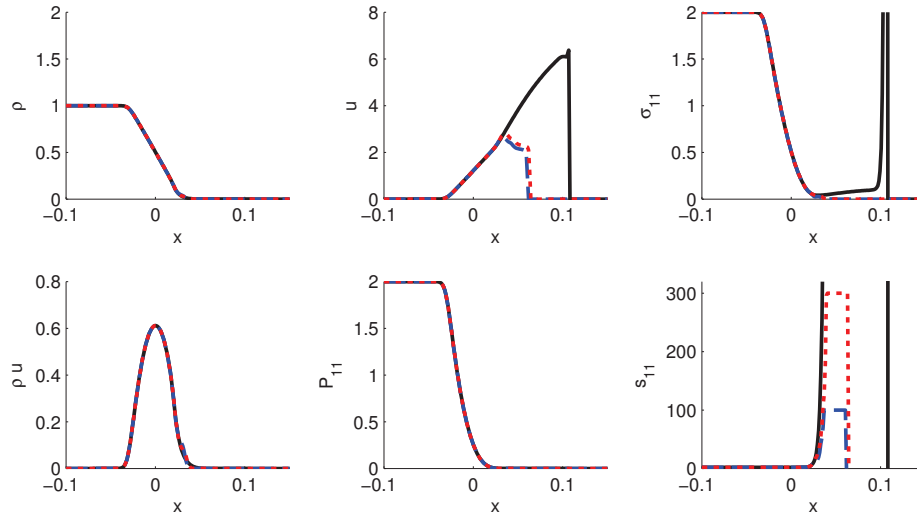


Figure 4: Riemann problem with vacuum at time $t = 0.05$ s: MUSCL/HLL scheme with 200 cells without limitation (black full line), with $S_{\max} = 100$ (blue dashed line) and with $S_{\max} = 300$ (red dotted line).

num entropy and twice the maximum entropy at $t = 0$. Both limited computations reproduce equivalent results for density momentum and pressure in comparison with the non-limited result. However central moments u and σ_{11} are now constrained, resulting in reasonable limitations on the time step. The effect on the entropy is also obvious, as the threshold is clearly the limit. A slight entropy oscillation appears at the initial state interface but it does not impact the accuracy on the full moments.

5 Eulerian simulation of two crossing jets

In the literature pressure-like models developed in the context of ACBMM have been tested in the context of turbulent flows [23, 40, 50, 51, 60, 64], where the turbulent mixing generates multiple and complex crossings. While such configurations are of particular interest for final turbulent applications, they do not assess the behavior of the model for the simplest crossing scenario: the crossing between two trajectories. This simple scenario is the building element of what happens in a turbulent case so we propose to set up a specific test case.

To investigate this scenario we consider a situation where the strain rate of the gaseous carrier field will generate PTC for the particulate phase. This test case has already been investigated in 1D in [19, 52], and here in its 2D version. By injecting particles in the gaseous field from two positions we will generate, depending on the relaxation time of the particles, a two-trajectory crossing. In the following we detail this configuration as well as its analytic Lagrangian solution. We thus analyze the results for the AG model, emphasizing on the description of the spatial distribution of the number density as well as on the energy budget.

5.1 Configuration description and analytical solution

We consider a carrier phase with the given velocity field in a Cartesian frame $(x, y) \in [0, H] \times [0, L]$:

$$\begin{pmatrix} u_g \\ v_g \end{pmatrix}(x, y) = \begin{pmatrix} u_{g0} \\ -\epsilon y \end{pmatrix}, \quad (5.1)$$

so that it flows constantly in the x -direction at a velocity u_{g0} from left to right but with a compressive velocity field in the y -direction i.e. velocities oriented towards $y=0$. The rate of strain on the $y=0$ axis of symmetry is $\epsilon = \left| \frac{\partial v_g}{\partial y}(y=0) \right|$. If we inject particles at time $t=0$ and at $x=0$ at the velocity $U_{p0} = u_{g0}$ and $V_{p0} = 0$ that is at equilibrium with the x -component of the gas velocity, they move uniformly in the x -direction. But they also accelerate in the y -direction and migrate towards the center according to the Lagrangian equations:

$$d_t Y_p = V_p, \quad d_t V_p = -\frac{1}{\tau_p}(V_p - v_g(Y_p)) = -\frac{1}{\tau_p}(V_p + \epsilon Y_p), \quad (5.2)$$

where Y_p and V_p are the Lagrangian position and velocity of a particle. Combining the Lagrangian equations yields a scalar second order equation that describes the y -motion in a frame that moves along the x -axis:

$$d_t^2 Y_p + \frac{1}{\tau_p} d_t Y_p + \frac{\epsilon}{\tau_p} Y_p = 0. \quad (5.3)$$

We define a Stokes number $St = \epsilon \tau_p$. We also define $\omega^2 = \frac{1}{4} \left| \frac{1}{\tau_p^2} - \frac{4\epsilon}{\tau_p} \right|$, and the critical Stokes number $St_c = \frac{1}{4}$ [19]. The solution is then given by:

$$Y_p(t) = Y_{p0} \exp\left(-\frac{t}{2\tau_p}\right) \begin{cases} \exp(-\omega t) & \text{if } St \leq St_c \\ \cos(-\omega t) + \frac{1}{2\omega\tau_p} \sin(-\omega t) & \text{otherwise.} \end{cases} \quad (5.4)$$

First, the particles converge towards the center in a characteristic time that is $2\tau_p$. Second, if particles are injected at least two different ordinates Y_{p1} and Y_{p2} , PTC occurs as soon as oscillation occurs that is $St > St_c$.

When multiplying Eq. (5.3) by velocity, one gets after integration an equation on the specific energy of a particle:

$$\frac{D}{Dt} \left(\frac{\dot{Y}_p^2}{2} + \frac{\epsilon}{\tau_p} \frac{Y_p^2}{2} \right) = -\frac{1}{\tau_p} \dot{Y}_p^2, \quad (5.5)$$

where one recognizes a kinetic energy $e_c = \frac{1}{2} \dot{Y}_p^2$ and a potential energy $e_p = \frac{\epsilon}{2\tau_p} Y_p^2$. The latter comes from a part of the drag force, which has been split in a conservative and a non-conservative part. The potential is high when particles are far from the centerline

and minimum when particles are at the center. The sum of these two energies is the mechanical energy that decreases due to the non-conservative part of the drag force.

We finally define two tools dedicated to the analysis of the two-jet configuration: the y -integration operator and the notion of orbitals. To quantitatively compare the different approaches we define the y -integration operator over a quantity \cdot :

$$\langle \cdot \rangle_y = \int_{y_0}^{y'} \cdot dy', \quad (5.6)$$

where y_0 is the y -ordinate of the centerline. The cumulative number density reads:

$$\psi(x, y) = \frac{\langle \rho(x, y') \rangle_y}{\langle \rho(x, y') \rangle_{+\infty}}, \quad (5.7)$$

and is a number (per square length). An $\alpha\%$ -orbital is then defined as a sub-manifold of the $x-y$ plane containing the center line and which encloses $\alpha\%$ of the total number of particles at every x -position.

5.2 Eulerian simulation

We now consider a domain $H = 2$ m and $L = 6$ m. The mesh is 1000×400 cells. The gas flow has an x -velocity $U_g = 0.2$ m/s and a y -strain $\epsilon = 1$ s⁻¹. Two particle jets of width $\delta = 0.2$ m are injected at y -ordinates $y_1 = 0.5$ m and $y_2 = 1.5$ m with $U_{l, inj} = U_g = 0.2$ m/s and $V_{l, inj} = 0$. The particle Stokes number is $St = 5 = 20St_c$, which is sufficient to let PTC occur. The entropy limitation is used with $S_{max} = 1$.

In Fig. 5 the steady solution of the AG model is represented. The white lines represent the limits of the analytical solution described by Eq. (5.4). Results show that even if before the first crossing Lagrangian and Eulerian are in very good agreement, after the first crossing, the AG solution is distributed between the two extremal Lagrangian orbitals. However the number density is still enclosed, and reproduces the length scales (amplitude and spacing) of the crossing even if it cannot capture the details of it.

After the first crossing, the AG model loses the detailed information of the velocity distribution, projecting it with respect to the second order moments onto the maximum entropy distribution (in the information sense). In fact, it destroys the information that is not reproduced by the reconstructed NDF. To exhibit this information loss, we propose to replace the two jets by one jet which as a Gaussian spatial distribution in the y -direction. Therefore the injection condition at $x=0$ is described by the following spatial distribution:

$$\rho_{inj}(y) = \frac{2\delta}{\sqrt{2\pi\sigma_{inj}}} \exp\left(-\frac{(y-1)^2}{2\sigma_{inj}}\right), \quad \sigma_{inj} = \int_0^H \rho(y) U_{p0} dy. \quad (5.8)$$

Results for the Gaussian injection are represented in Fig. 6. Again white lines represent the extremal orbitals of the Lagrangian solution. Here before the first crossing the Eulerian and Lagrangian solutions are no longer equivalent. After the first crossing however,

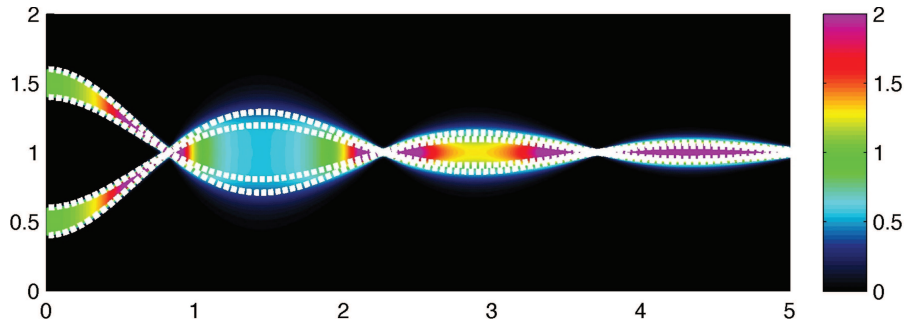


Figure 5: Steady solution of two inertial particle jets ($St=20$) injected in a compressive velocity field: particle number density (m^{-3}). White lines represent the lower and upper Lagrangian trajectories for each jet.

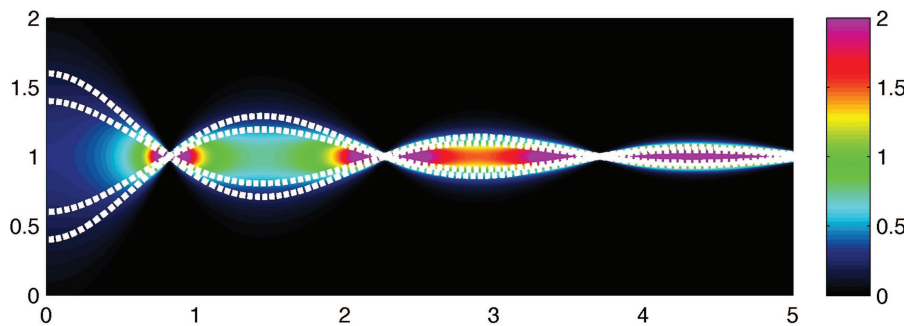


Figure 6: Steady solution of Gaussian particle jet ($St=20$) injected in a compressive velocity field: Particle number concentration (m^{-3}). White lines represent the lower and upper Lagrangian trajectories for each jet.

the Eulerian solution of the Gaussian jet becomes similar to the one of the two-jet configuration:

- Most of the number density is enclosed in-between the Lagrangian trajectories;
- Internal energy is generated at each crossing events.

The Gaussian jet and the two-jet configurations look similar after the first crossing, which has destroyed a part of the information of the injection conditions.

We can estimate the number of particles that are enclosed in-between two y -ordinates thanks to the y -integral defined in Eq. (5.6). Since the problem is symmetric, $\psi(x,y)$ is also symmetric in the y -direction. Results are represented in Fig. 7. As qualitatively assessed, before the first crossing, the two-jet configuration locates the number density well, while the Gaussian injection condition results in a spreading. After the first crossing both injection conditions give a smeared solution. The 80%-orbitals are the same, close to the extremal orbitals of the Lagrangian solution. The 99%-orbitals differ after the first crossing, but they end up to be similar after the second crossing. Thus both two-jet and Gaussian-jet configurations become equivalent in terms of number density after crossing.

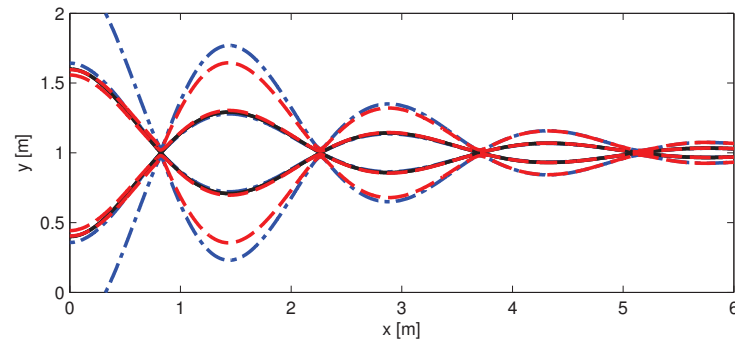


Figure 7: Statistics of the jet configurations into a gaseous compressive field: isolines of cumulative number density for the two-jet analytical solution (100%, black line), the two-jet AG solution (80% and 99%, red lines), and the Gaussian-jet AG solution (80% and 99%, blue lines).

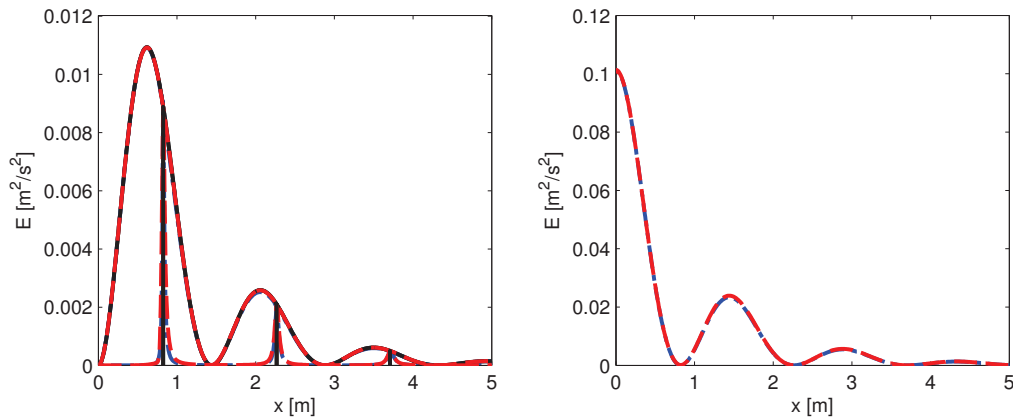


Figure 8: Statistics of the jet configurations into a gaseous compressive field: mean and internal energies (left, the upper curves are for mean energy, the lower for internal energy), and potential energy (right) for the Lagrangian solution (black continuous line), the AG solution of the two-jet (red dashed line) and the Gaussian jet (blue dot-dashed line) configurations.

To further analyze the behavior of the model on both configurations, the mean, integral, and potential density-weighted energies integrated over the y -direction are plotted against the x -direction in Fig. 8. Results show that the evolution of the energy is reproduced with a good precision compared to the Lagrangian solution. Even before the first crossing, two-jet and Gaussian-jet configurations are identical. It demonstrates that the AG model preserves the information of the second order moments at each crossing event, discarding any higher order information such as the third order central moments.

5.3 Conclusion on the model

In conclusion of this test case results demonstrate the main drawback of the AG model: it cannot capture the density distribution generated by deterministic crossings such as in

the present configuration. However, when the crossing is generated because of the drag force of a straining gaseous flow field, the particle trajectories are enclosed in manifolds that correspond to a specific space scale. The AG model is able to reproduce this scale, and it captures the width of the crossing and its energetic behavior. Another interesting property of the AG model is that, after a crossing it does not allow to determine if the crossing has been generated by a deterministic event, such as a two-jet crossing, or an ensemble of initial/boundary conditions totalizing the same zero, first and second order spatial moments.

6 Application to vortex and turbulent flow fields

The ability of the model to reproduce one crossing event being evaluated, we investigate two more complex cases where several crossing events are encountered:

- The 2D Taylor-Green vortices: this test case features four contra-rotative vortices with periodicity. It is interesting because it is composed of one scale, and the conditions for PTC are easy to determine. Furthermore the Lagrangian solution exhibits different structures that correspond to simple or multiple crossings that are of interest for real turbulent flows. It is an intermediate case between laminar and fully turbulent cases, because in a turbulent field, the particulate phase will interact with a full spectrum of scales, each of them having a specific interaction with the particles. Finally it is also a good test case to demonstrate the quality of the numerics.
- The 2D Decaying Homogeneous Isotropic Turbulence: the physics of this test case is relevant for realistic applications. The turbulence of the carrier phase generates multiple crossing events everywhere in the domain that are impossible to treat separately in the Eulerian vision of the flow: the validation of Eulerian strategies requires to investigate their ability to treat such superimposed scales. The first level of real turbulent flows is the Homogeneous Isotropic Turbulence, for which the spectrum of scales is well-known. Moreover, we choose a decaying turbulence to assess the interaction of particles with unsteady time scales.

In the following, we will compare the AG model to a Lagrangian solution with 10 million particles. We will also investigate the importance of the anisotropy of the model by comparing to the results of the Isotropic Gaussian model. Actually this model is obtained by assuming that the energy tensor Σ is isotropic, leading to the Euler equations. This model is the simplest one that can be used to reproduce PTC. Its main advantage is that less moments are solved, as only one second order moment is needed: the total energy. However, as it has been shown in the two-crossing jet case, crossing events are highly anisotropic, and this model could reveal to be inaccurate.

To analyze the results, we will use two tools:

- Instantaneous fields: first, the spatial distribution of particles is investigated. This is the primary information that we want to capture, and the two-jet case has shown

that the AG is not able to reproduce details, but can capture scales of the flow. We then want to verify if it is still the case in turbulent-like conditions, where multiple crossing events can be found at each location.

- **Statistics:** to evaluate quantitatively the ability of the Eulerian approaches to reproduce the Lagrangian reference, three statistics of the flow are investigated: the segregation, the mean central energy and the mean total energy. The segregation evaluates the generation of stiff accumulation and vacuum zones. It is of particular importance, for example for dense flows, where the local concentration is a leading term to evaluate the coalescence source term, or for the combustion of droplets, where the inhomogeneity of the droplet phase highly influences the whole process. Mean total and central energies are also helpful to determine if the coupling between the gas and the particle phases is well resolved. Here we evaluate the statistical quantities on a fixed reference mesh of 64^2 cells on which all results are projected, for which Lagrangian results are statistically converged. They are expressed as:

$$g_{pp} = \frac{\{\rho^2\}}{\{\rho\}^2}, \quad \delta\tilde{\Theta}_p = \frac{\{\rho(\sigma_{11} + \sigma_{22})\}}{2\{\rho\}}, \quad \tilde{E}_p = \frac{\{\rho(E_{11} + E_{22})\}}{2\{\rho\}}, \quad (6.1)$$

where g_{pp} is the segregation, $\delta\tilde{\Theta}_p$ the mean central energy, \tilde{E}_p the mean total energy, and $\{\cdot\}$ the spatial averaging operator over the whole domain using the quantities projected on a 64^2 -cell mesh.

6.1 Taylor-Green vortices

The gas velocity field of the TG is the following:

$$u_g(x,y) = \sin(2\pi x)\cos(2\pi y), \quad v_g(x,y) = -\cos(2\pi x)\sin(2\pi y). \quad (6.2)$$

The dynamics of particles generated by a drag coupling with TG is characterized by a critical Stokes number $St_c = 1/8\pi$ as defined in [19]. Below this limit particles stay in their initial vortex and do not encounter PTC. Above this limit particles have a sufficient inertia to leave their initial vortex. They will generate PTC, which scales become larger as the Stokes number increases. In the following we will investigate TG for three Stokes numbers: $St = St_c$, $5St_c$, and $10St_c$. The solution obtained by a Lagrangian Tracking is considered as the reference. Isotropic (IG) and Anisotropic Gaussian (AG) closures will be investigated, to highlight the importance of the central energy partition in each direction that is done by AG and not by IG. If it is not mentioned the mesh size is composed of 256^2 equi-distributed cells.

6.1.1 Instantaneous fields

First the number density field obtained at time $t = 4$ is compared for each method and each Stokes number (Figs. 9-11). At $St = St_c$, the number density fields have the same

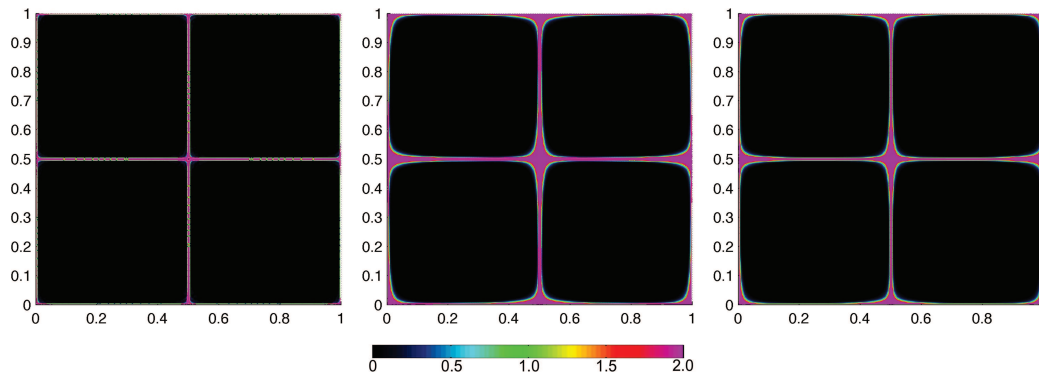


Figure 9: Taylor Green Vortices for $St=St_c$: number density field at time $t=4$ for the Lagrangian tracking (left), for the Eulerian Isotropic Gaussian closure (center), and for the Eulerian Anisotropic Gaussian closure (right).

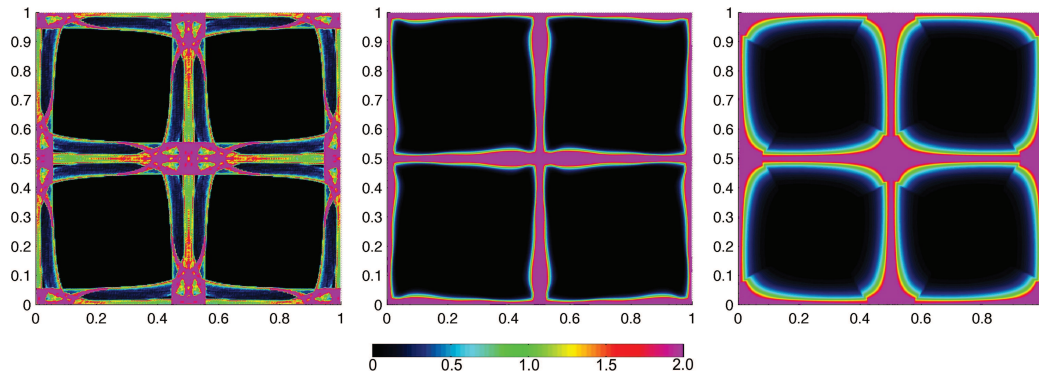


Figure 10: Taylor Green Vortices for $St=5St_c$: number density field at time $t=4$ for the Lagrangian tracking (left), for the Eulerian Isotropic Gaussian closure (center), and for the Eulerian Anisotropic Gaussian closure (right).

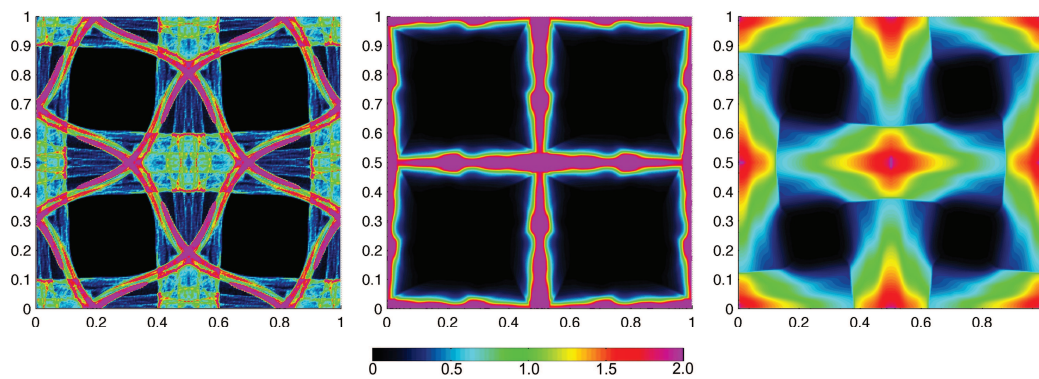


Figure 11: Taylor Green Vortices for $St=10St_c$: number density field at time $t=4$ for the Lagrangian tracking (left), for the Eulerian Isotropic Gaussian closure (center), and for the Eulerian Anisotropic Gaussian closure (right).

structure for each simulation i.e. a stiff accumulation of particles in the lowest vorticity zones. Eulerian solutions (IG and AG) are equivalent, which is expected because at this Stokes number no PTC occurs. This implies that no central energy is generated and the two models behave like the Monokinetic model [19, 42]. Compared to the Lagrangian reference the two Eulerian models feature a diffused solution[§].

At $St = 5St_c$ PTC is expected so the model will generate a central energy. Contrary to $St = St_c$ the number density field are different for each model at $St = 5St_c$. In Fig. 10 the structures generated by each simulation are relatively different. At this Stokes number, the Lagrangian reference generates two types of structures: four stiff equilibrium manifolds (EM) out of the low vorticity zones, which are the long-time solution of the particle system of ODEs in TG and larger mixing zones where droplets are traveling around the low vorticity zones without being attracted inside one of the equilibrium manifolds. The two Eulerian approaches are able to capture the mixing zones but do not reproduce the EM. To capture the EM, an Eulerian approach must be able to reproduce exactly the PTC between two trajectories, which is not the case for one-velocity-node Eulerian approaches[¶]. Finally even if IG and AG solutions are different, the best solution among the Eulerian approaches cannot be discriminated by solely considering the number density field. However looking at the results for $St = 10St_c$ clearly shows that the IG closure no longer reproduces the characteristic width of the mixing zones, contrary to AG.

6.1.2 Statistics

In the following of the two-jet crossing case, we further investigate the behavior of our models by means of statistical quantities namely the segregation and the energy budget. Statistics are plotted in Figs. 12-14 for $St = St_c$, $5St_c$, and $10St_c$.

At $St = St_c$, the segregation is high due to the accumulation of particles in low vorticity zones. The mean central energy is relatively small compared to the mean total energy. Both IG and AG reproduce the profile of the time evolution but they do not recover the same levels. Both models underestimate the segregation, AG giving the best result compared to the Lagrangian reference. The mean central energy is well captured by both approaches but the mean total energy is better captured by AG, which can be directly linked to the segregation results: as we consider phase-average values, missing the description of the segregation will limit the ability to capture the mean total energy, which is also sensitive to the segregation.

At $St = 5St_c$ the AG captures well all the statistics under study, whereas the IG overestimates the segregation. This is a consequence of the underestimation of the mean central energy: actually, the internal energy generates the width of the structures and in the case of IG this energy is too small to capture the correct width.

At $St = 10St_c$, the IG closure again strongly overestimates the segregation, whereas the AG leads to good results but for a short time only. In terms of energy, the results of AG

[§]But the diffusion length decreases with the mesh refinement.

[¶]In [43, 78] more nodes have been used and it permits to capture such structures.

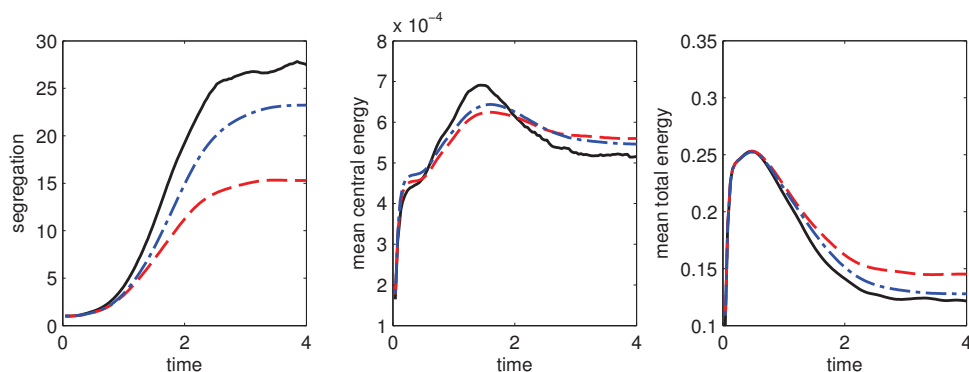


Figure 12: Taylor Green Vortices for $St=St_c$: time evolution of the segregation (left), mean central energy (center), and mean total energy (right) for the Lagrangian tracking (black full line), the Eulerian Isotropic (red dashed line) and Anisotropic (blue dot-dashed line) Gaussian closures.

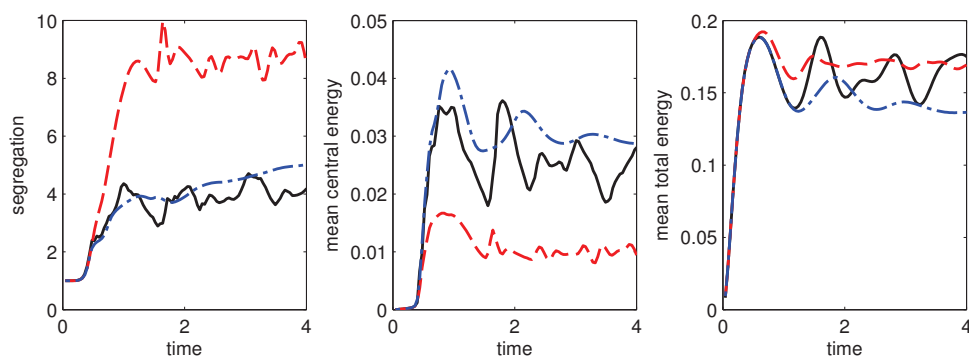


Figure 13: Taylor Green Vortices for $St=5St_c$: time evolution of the segregation (left), mean central energy (center), and mean total energy (right) for the Lagrangian tracking (black full line), the Eulerian Isotropic (red dashed line) and Anisotropic (blue dot-dashed line) Gaussian closures.

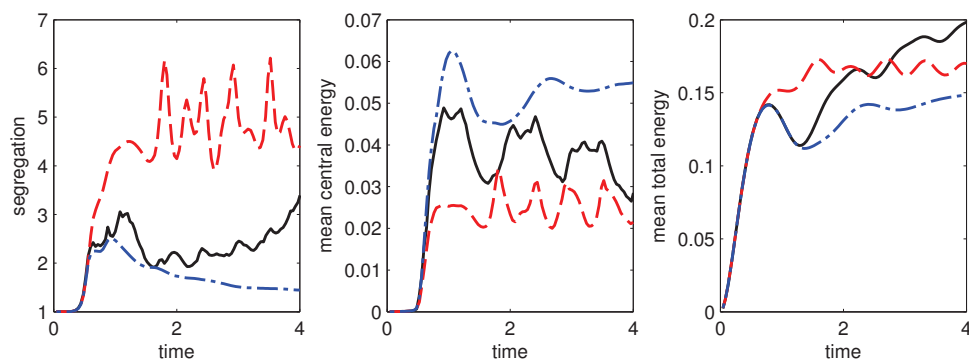


Figure 14: Taylor Green Vortices for $St=10St_c$: time evolution of the segregation (left), mean central energy (center), and mean total energy (right) for the Lagrangian tracking (black full line), the Eulerian Isotropic (red dashed line) and Anisotropic (blue dot-dashed line) Gaussian closures.

are again only predictive for a short time, the long-time behavior being missed by both Eulerian approaches.

To conclude on the TG case, compared to the Lagrangian reference the AG gives better results than the IG, because the anisotropy of the velocity distribution is mandatory to reproduce the directional information within PTC zones. In terms of instantaneous field or statistics, AG leads to satisfactory results for moderate Stokes number but at high Stokes number the method becomes less predictive.

6.2 Decaying Homogeneous Isotropic Turbulence

The Homogeneous Isotropic Turbulence (HIT) case is closer to real applications. The gaseous flow field consists in a full spectrum of space and time scales, whereas TG has a unique and steady one, and is time-evolving so that the large-scale sweeping of small scales is present. Such a case is a mandatory step for each modeling method before going to more complex applications and is extensively investigated in the literature [29, 40, 57, 66, 79].

Here we consider a flow field generated by the ASPHODELE code, developed at CO-RIA by Julien Réveillon and collaborators [59]. All quantities are dimensionless. The domain is 3×3 . The parameters of the turbulent field at $t=0$ are listed in Table 3.

Table 3: Turbulence properties at time $t=0$.

Re_t	u_t	ϵ	η_K	l_{int}	τ_K	τ_{int}
7.12	0.1	0.01	0.022	0.1	0.36	1.0

In the following the Stokes number will be considered as the ratio of the relaxation time of particles to the Kolmogorov time scale at $t=0$: $St = \frac{\tau_p}{\tau_K}$. This Stokes number is the most relevant in our case, as we will start with equal velocities for gas and disperse phases at $t=0$, so that crossings are generated at time $t=0$. Similarly to TG case, we investigate instantaneous solutions as well as space-average statistics.

6.2.1 Instantaneous fields

The instantaneous flow field at time $t=3.6$ is plotted in Figs. 15-16 for $St=1$, and 10. Similarly as in the TG case, negligible PTC is expected at $St=0.75$ and the two Eulerian simulations therefore give similar results, all comparable to the Lagrangian reference though being more diffusive. At $St=10$, the Lagrangian result exhibits mixing zones like in the TG case, where particles oscillate around the low vorticity zones, but no long-time equilibrium manifolds, which cannot be captured by IG or AG. The two Eulerian approaches capture the mixing zones, but their widths are closer to the Lagrangian ones with the AG model.

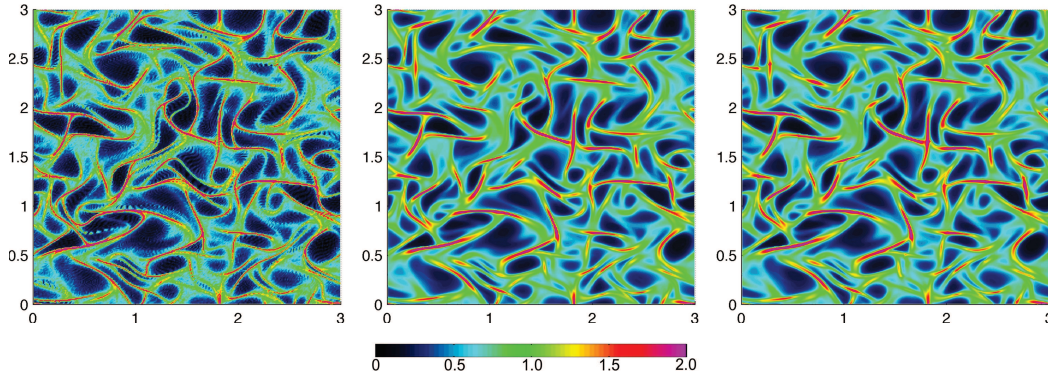


Figure 15: HIT case for $St=1$: number density field at time $t=3.6$ for the Lagrangian tracking (left), for the Eulerian Isotropic Gaussian closure (center), and for the Eulerian Anisotropic Gaussian closure (right).

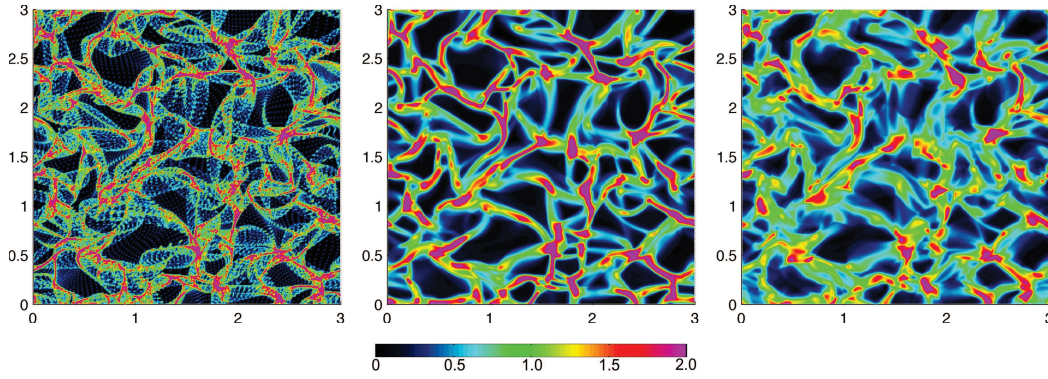


Figure 16: HIT case for $St=10$: number density field at time $t=3.6$ for the Lagrangian tracking (left), for the Eulerian Isotropic Gaussian closure (center), and for the Eulerian Anisotropic Gaussian closure (right).

6.2.2 Statistics

We investigate the same statistics as in the TG case, i.e. the segregation, the mean central energy, and the mean total energy. For $St=1$ the two Eulerian models give the same results. The comparison with the Lagrangian reference is satisfactory, even if the segregation is slightly underestimated. For $St=10$ the two models give now different results. The AG model underestimates the segregation while overestimating the mean central energy, whereas the IG model has an opposite behavior. However the mean total energy is well reproduced only by the AG model.

To better estimate the quality of the model we perform in Fig. 19 a mesh sensitivity analysis for all statistics at $St=10$. Compared to the TG case where the generated scales of the particulate phase are relatively wide, the scales generated by the HIT case are small compared to the mesh size. The results show that refining the mesh, thus reducing the numerical diffusion, tends to increase the segregation and to decrease the mean central energy. Whereas the mesh refinement degrades the IG results, AG results are closer and

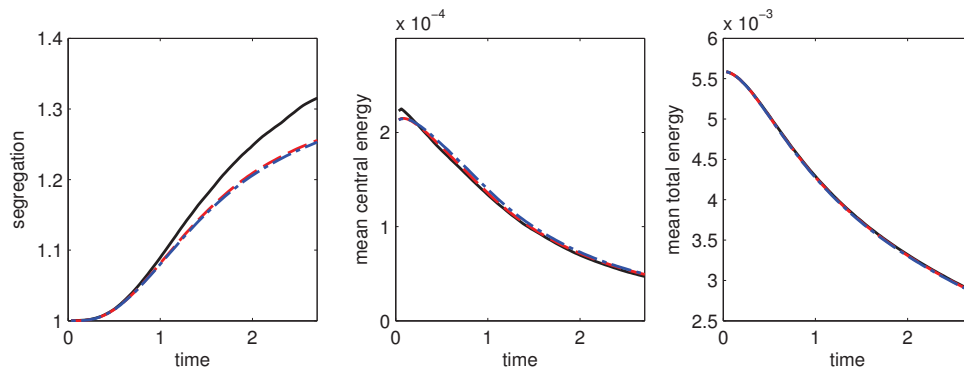


Figure 17: HIT case for $St=1$: time evolution of the segregation (left), mean central energy (center), and mean total energy (right) for the Lagrangian tracking (black full line), the Eulerian Isotropic (red dashed line) and Anisotropic (blue dot-dashed line) Gaussian closures.

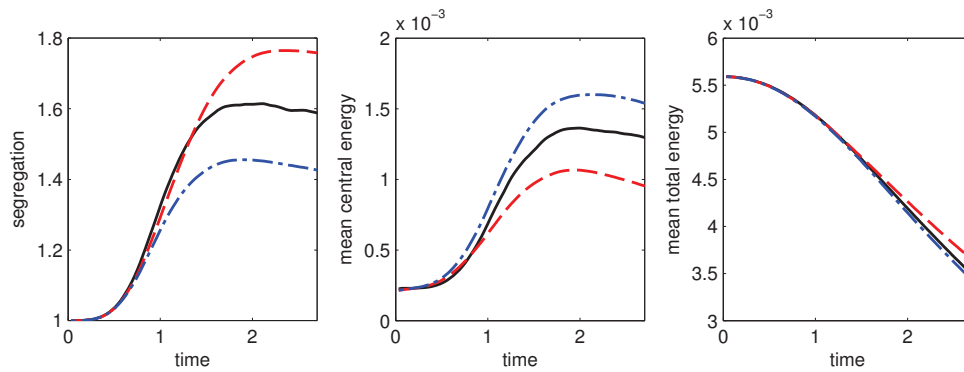


Figure 18: HIT case for $St=10$: time evolution of the segregation (left), mean central energy (center), and mean total energy (right) for the Lagrangian tracking (black full line), the Eulerian Isotropic (red dashed line) and Anisotropic (blue dot-dashed line) Gaussian closures.

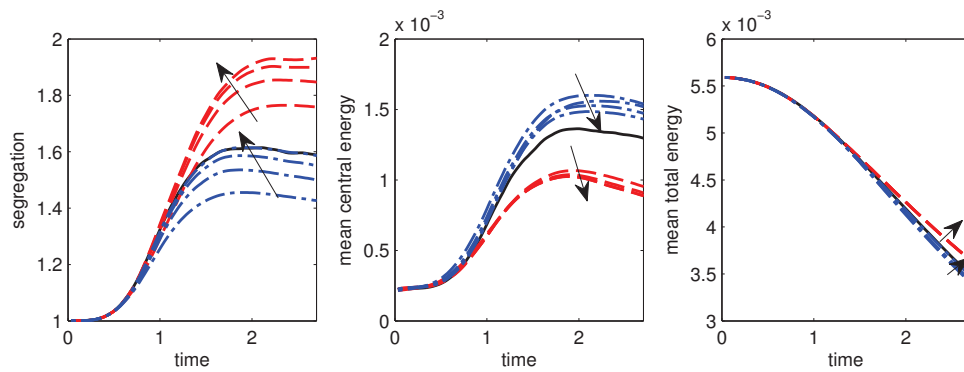


Figure 19: HIT case for $St=10$, impact of the mesh on statistics: time evolution of the segregation (left), mean central energy (center), and mean total energy (right) for the Lagrangian tracking (black full line), the Eulerian Isotropic (red dashed line) and Anisotropic (blue dot-dashed line) Gaussian closures. Arrows indicates growing meshes for each Eulerian model (from 256^2 to 2048^2 cells).

closer to the Lagrangian results, confirming the mesh convergence of the results. It also clearly shows the importance of the numerical methods for Eulerian models: second order schemes are a minimum requirement for turbulent computations. Less dissipative second order schemes based on Discontinuous Galerkin methods are in development [41,62] and higher order schemes could be envisioned.

7 Conclusion

In this work a new method of moments for particle-laden flows, the 10-moment Anisotropic Gaussian model, together with the principles of KBMM for the modeling of such flows, is introduced. This method of moments up to second order has already been used in the context of rarefied gases [12, 46, 55] and is here extended to the simulation of particle-laden flows. Relying on previous works by [36] and [2] this approach is not only introduced to provide a closure of the system of conservation laws at the moment level but also allows, based on entropy maximization in both information and kinetic senses, to obtain a model for particle-laden flows with realizability as well as an entropic structure. Moreover the resulting moment system is hyperbolic, entitling the use of Godunov solvers [44,68]. To ensure robust and accurate simulations a MUSCL/HLL scheme has been proposed, based on a linear reconstruction of primitive variables and a proper limitation strategy to keep the boundary values realizable. It results in a stable, realizable, and accurate scheme for the transport of particles, which is usually a stumbling block for most Eulerian moment models.

The modeling approach and numerical scheme have been validated on 1D cases, to highlight the accuracy of the scheme for regular and shocked solutions, as well as important features of the model. Moreover the importance of a regularization procedure at interfaces achieving vacuum has been shown, with a limited impact on the accuracy of the model.

Then an injection case into a compressive gaseous carrier flow field has been investigated. Such a configuration couples transport and drag in such a way that the fluid particle phase can be considered as hypercompressible^{||} for a range of Stokes number involving inertial particles. This case provides of good model for PTC generation in turbulent flows. Results show that the AG model is not able to reproduce the details of deterministic crossings in terms of number density spatial distribution. However it captures at least the right scale and the right energetic behavior. Moreover, an important aspect of this model is that, after a crossing event, it “destroys” part of the information before the crossings, only keeping the information on zero-to-second order moments in space. Thus the spatial behavior of this model is directly linked to the velocity phase space description.

^{||}Hypercompressibility is defined properly in [20] and is related to the fact that the divergence of the velocity field of the particles, obtained from the first order moment divided by the zeroth order moment, can grow and become singular during an occurrence of PTC.

Finally the AG model has been evaluated on 2D turbulent-like test cases. Both Anisotropic and Isotropic Gaussian closures have been compared and we have shown the importance of having a full description of the pressure tensor in order to properly predict the segregation of particles, a key feature for combustion application for example. In the Taylor Green vortices the two Eulerian models are not able to get the details of the spatial distribution. However as in the injection case the AG model captures the characteristic scales of the flow, where IG cannot. In the decaying turbulence the AG model renders a more relevant segregation than IG. Moreover a mesh sensitivity analysis shows that the AG results reproduce the Lagrangian solution, whereas IG does not. The partition between mean and internal energies is also better captured by the AG model and the mesh sensitivity analysis again demonstrates that AG model reproduces the Lagrangian solution.

In conclusion the AG model in conjunction with the accurate MUSCL/HLL scheme that has been proposed are an interesting robust strategy for the simulation of particle-laden flows. However, some aspects of the results have to be understood as consequences of the modeling approach: such a presumed-velocity-PDF approach is not supposed to capture the full range of scales but to reproduce some statistical quantities correctly at the scale of the crossings. Moreover the impossibility to make the difference between deterministic crossings and the variability imposed by initial/boundary conditions after the crossing event has to be kept in mind in the interpretation of the results. It has also been shown that such an approach is robust for shear layers, compared to ACBMM methods [75].

Let us finally underline a few issues that still need to be addressed before the model is ready for realistic applications, thus showing the level of maturity of the proposed model and numerical methods. These issues are the following:

- It would be desirable to compare such a numerical approach to a relaxation approach in the spirit of [9] for the AG system of conservation laws and draw firm conclusions on what is the best-suited method for realistic configurations in terms of both computational cost and accuracy,
- The problem of the interface with vacuum zones has to be further investigated. The use of a first order entropy-preserving HLL scheme is not sufficient to guarantee bounded entropy in this context. The present work handles these interfaces by using a limitation procedure using a user-defined case-dependent parameter. To free the simulation of such a parameter, a discrete-entropy-diminishing scheme in the presence of vacuum has to be designed, as well as a clear understanding of the behavior of the numerics in such zones.
- We are headed towards tackling 3D configurations and higher Reynolds numbers,
- Investigating a higher order scheme that preserves realizability on unstructured meshes is desirable [61,62] but relies on a detailed study of multi-dimensional properties of the associated system of conservation laws and entropic structure.

- The potential of our approach for the LES of complex configurations has also to be assessed. Actually, the ACBMM equivalent of our model (see [50,51] and references therein) is routinely used for LES of real applications [49,63,72]. However, before going to the real applications, fundamental studies about the definition of a fully realizable KBMM-LES moment method have to be conducted in the spirit of [17,81].
- In a case where the details of the deterministic crossings are mandatory, the reader may refer to other contributions using a Multi-Gaussian closure [15,43,71]. Another important aspect is also the ability to switch from one model to the other depending on the complexity of the crossing or the requirement we have on its representation. Such a topic is addressed in [9], by switching between pressureless and Gaussian models depending on the occurrence of crossing. This work will be extended to Anisotropic Gaussian and Multi-Gaussian closure in future works.

Acknowledgments

The authors would like to thank the SAFRAN group, which sponsored the stay of Aymeric Vié during the Summer Program 2012 at Center for Turbulence Research (CTR), Stanford University, as well as the CTR for the technical support. The support of the France-Stanford Center for Interdisciplinary Studies through a collaborative project grant (PIs: P. Moin and M. Massot) is also gratefully acknowledged. The authors also thank ONERA and DGA, Ministry of Defence (M. S. Amiet, Technical Monitor) for François Doisneau's PhD Grant. The post-doctoral stay of A. Vié has also been supported by the ANR Sechelles (PIs S. Descombes and M. Massot) and DIGITEO Project (PI M. Massot). We finally thank Frédérique Laurent-Nègre for her comments and revisions, Joel Dupays for useful discussions and O. Simonin for fruitful discussions which have motivated the writing of Section 2.2.

A Size-conditioned extension

In the present appendix we show how AG can be extended to a polydisperse phase. In the literature, polykinetic approaches have been extended using Multi-Fluid approaches (MF, [38,42,72]). We show that it is always possible to extend polykinetic approaches with MF, as long as the velocity distribution is size-conditioned:

$$g(t, \mathbf{x}, \mathbf{c}, S) = f(t, \mathbf{x}, \mathbf{c} | S) h(t, \mathbf{x}, S),$$

where S is a particle size variable and $h(t, \mathbf{x}, S)$ is a probability density function of unity integral. We consider an extended Williams-Boltzmann equation with additional terms in the size phase space:

$$\partial_t g + \mathbf{c} \cdot \partial_{\mathbf{x}} g + \partial_{\mathbf{c}} \cdot (\mathbf{F}g) + \partial_S (R_S g) = 0, \quad (\text{A.1})$$

where R_S is a velocity in the size space, for instance linked to evaporation. Integrating Eq. (A.1) over the velocity space, we get the semi-kinetic system [19]:

$$\partial_t M_{i,j,k|S} h(S) + \partial_x \cdot h(S) \begin{pmatrix} M_{i+1,j,k|S} \\ M_{i,j+1,k|S} \\ M_{i,j,k+1|S} \end{pmatrix} = \frac{h(S)}{\tau_p(S)} \left((i+j+k) M_{i,j,k|S} - u_g \cdot \begin{pmatrix} i M_{i-1,j,k|S} \\ j M_{i,j-1,k|S} \\ k M_{i,j,k-1|S} \end{pmatrix} \right) - \partial_S R_S M_{i,j,k|S} h(S). \quad (\text{A.2})$$

In this system, if one size S is considered, the moment equations of AG are recovered, with an additional size space flux. If we also want to use a moment method for the size space, MF can be used. By considering size intervals $[S_l, S_{l+1}]$ for $l=0, \dots, N$ to map the compact support $S \in [0, S_{\max}]^{**}$, sectional size-velocity moments can be defined:

$$M_{i,j,k}^l = \frac{1}{S_{l+1} - S_l} \int_{S_l}^{S_{l+1}} h(S) M_{i,j,k|S} dS. \quad (\text{A.3})$$

By considering a first order piecewise constant distribution in size $h(S) = 1$, and that the size conditioned velocity moments are evaluated at the size cell midpoint $S_{m,l} = (S_l + S_{l+1}/2)/2^{++}$, we get $M_{i,j,k}^l = M_{i,j,k|S_{m,l}}$. The final Multi-Fluid AG system is then obtained:

$$\partial_t M_{i,j,k}^l + \partial_x \cdot \begin{pmatrix} M_{i+1,j,k}^l \\ M_{i,j+1,k}^l \\ M_{i,j,k+1}^l \end{pmatrix} = \frac{1}{\tau_p(S_{m,l})} \left((i+j+k) M_{i,j,k}^l - u_g \cdot \begin{pmatrix} i M_{i-1,j,k}^l \\ j M_{i,j-1,k}^l \\ k M_{i,j,k-1}^l \end{pmatrix} \right) - \frac{1}{S_{l+1} - S_l} \left(R_S M_{i,j,k|S_{l+1}} - R_S M_{i,j,k|S_l} \right), \quad (\text{A.4})$$

the last term corresponding to fluxes in size phase space, that depend on size cell interface values. This term is evaluated using an upwind scheme, so that in the case of $R_S \leq 0$ (evaporation for instance):

$$\frac{1}{S_{l+1} - S_l} \left(R_S M_{i,j,k|S_{l+1}} - R_S M_{i,j,k|S_l} \right) = \frac{1}{S_{l+1} - S_l} \left(R_S M_{i,j,k}^{l+1} - R_S M_{i,j,k}^l \right). \quad (\text{A.5})$$

This method has been applied to coalescing flows [22] and further works will also extend the AG formulation to moment methods in size, as in [73, 74].

B Slope evaluation strategy

In the following a slope evaluation strategy is proposed which respects all the realizability constraints for the flux evaluation at the cell interfaces. Here we consider the 2D case,

** A semi-open support $S \in [0, +\infty[$ can also be considered by adding a last semi open section $[S_N, +\infty[$ [21, 24].

+++ This approximation is helpful to close the system but it can be relaxed using more complex methods [74]. For a first order method however this approximation has no impact on the accuracy of the method.

but the same rationale can be used to extend it to a slope limitation in a 3D case. The main idea of our limitation strategy is to define sufficient conditions for realizability, starting from the fact that a zero-slope reconstruction is always realizable. Thus, our rationale is to first evaluate the slope using a classical minmod-limiter, and then to apply a second limitation that reduces the slopes until realizability is reached. Thus, our reconstruction strategy can be applied in 3D in a straightforward manner.

First we treat the density to which a minmod limiter is applied with an additional positivity constraint:

$$D_{\rho_j} = \frac{1}{2} (\text{sign}(\rho_{j+1} - \rho_j) + \text{sign}(\rho_j - \rho_{j-1})) \min \left(\frac{\rho_{j+1} - \rho_j}{\Delta x}, \frac{\rho_j - \rho_{j-1}}{\Delta x}, \frac{2\rho_j}{\Delta x} \right). \quad (\text{B.1})$$

Second for the velocities, two types of constraints are imposed: a minmod limiter that takes into account the modification of the cell value [11] and two additional constraints to ensure the positivity of the energies:

$$D_{u_j} = \frac{1}{2} (\text{sign}(u_{j+1} - u_j) + \text{sign}(u_j - u_{j-1})) \min \left(\frac{|u_{j+1} - u_j|}{\Delta x(1 - \frac{D_{\rho_j} \Delta x}{\rho_j \frac{\Delta x}{6}})}, \frac{|u_j - u_{j-1}|}{\Delta x(1 + \frac{D_{\rho_j} \Delta x}{\rho_j \frac{\Delta x}{6}})}, D_{u_j}^{\max, \sigma_{11}} \right), \quad (\text{B.2})$$

where $D_{u_j}^{\max, \sigma_{11}} = \sqrt{\sigma_{11,j} / (\frac{\Delta x^2}{12} \alpha)}$. The slope on the velocity v being easily retrieved by analogy. Moreover the resulting slopes must keep the positivity of the corrected determinant within the cell:

$$\bar{\sigma}_{11,j} \bar{\sigma}_{22,j} - \bar{\sigma}_{12,j}^2 > 0. \quad (\text{B.3})$$

By developing each term we rewrite Eq. (B.3):

$$H = \sigma_{11} D_{v_j}^2 + \sigma_{22} D_{u_j}^2 - 2\sigma_{12} D_{u_j} D_{v_j} < \frac{\sigma_{11} \sigma_{22} - \sigma_{12}^2}{\frac{\Delta x^2}{12} \alpha}. \quad (\text{B.4})$$

If $H < 0$ the condition is always satisfied. If $H > 0$ and this condition is not fulfilled by the first slope evaluation, a correction factor $\gamma \in [0,1]$ is introduced:

$$D_{u_j}^{\text{new}} = \gamma D_{u_j}^{\text{old}}, \quad D_{v_j}^{\text{new}} = \gamma D_{v_j}^{\text{old}}, \quad \gamma = \min \left(1, \sqrt{\frac{\sigma_{11} \sigma_{22} - \sigma_{12}^2}{\frac{\Delta x^2}{12} \alpha H}} \right). \quad (\text{B.5})$$

Third, the slopes of the covariance matrix are evaluated. The following quantities are introduced to simplify the notations $\Sigma^* = \Sigma_j - \frac{\Delta x^2}{12} \alpha \mathbf{D}_{\mathbf{u}}^2$ and we impose a minmod slope evaluation that satisfies the positivity of the energies:

$$D_{\sigma_{11,j}} = \frac{1}{2} (\text{sign}(\sigma_{11,j+1} - \sigma_{11,j}) + \text{sign}(\sigma_{11,j} - \sigma_{11,j-1})) \min \left(\frac{|\sigma_{11,j+1} - \sigma_{11,j}|}{\Delta x(1 - \frac{D_{\rho_j} \Delta x}{\rho_j \frac{\Delta x}{6}})}, \frac{|\sigma_{11,j} - \sigma_{11,j-1}|}{\Delta x(1 + \frac{D_{\rho_j} \Delta x}{\rho_j \frac{\Delta x}{6}})} \right). \quad (\text{B.6})$$

This limitation does not ensure the positivity of the determinant, which is a quadratic function of the position:

$$\Delta(x) = \bar{\sigma}_{11}\bar{\sigma}_{22} - \bar{\sigma}_{12}^2 + \left(\bar{\sigma}_{11}D_{\sigma_{22,j}} + \bar{\sigma}_{22}D_{\sigma_{11,j}} - 2\bar{\sigma}_{12}D_{\sigma_{12,j}}\right)x + \left(D_{\sigma_{11,j}}D_{\sigma_{22,j}} - D_{\sigma_{12,j}}^2\right)x^2 > 0. \quad (\text{B.7})$$

After developing each term we finally get:

$$\Delta^* + A \left(x - \frac{\Delta x^2}{12} \frac{D_{\rho_j}}{\rho_j}\right) + B \left(x - \frac{\Delta x^2}{12} \frac{D_{\rho_j}}{\rho_j}\right)^2 > 0 \quad (\text{B.8})$$

with:

$$\Delta^* = \sigma_{11}^* \sigma_{22}^* - (\sigma_{12}^*)^2, \quad A = \sigma_{11}^* D_{\sigma_{22,j}} + \sigma_{22}^* D_{\sigma_{11,j}} - 2\sigma_{12}^* D_{\sigma_{12,j}}, \quad B = D_{\sigma_{11,j}} D_{\sigma_{22,j}} - D_{\sigma_{12,j}}^2. \quad (\text{B.9})$$

As the goal of the reconstruction strategy is to evaluate the value at the cell interfaces, we impose a weaker condition than Eq. (B.8):

$$\Delta^* + A \left(\pm \frac{\Delta x}{2} - \frac{\Delta x^2}{12} \frac{D_{\rho_j}}{\rho_j}\right) + B \left(\pm \frac{\Delta x}{2} - \frac{\Delta x^2}{12} \frac{D_{\rho_j}}{\rho_j}\right)^2 > 0. \quad (\text{B.10})$$

A new correction factor $\beta \in [0,1]$ is introduced:

$$D_{\sigma_{11,j}}^{new} = \beta D_{\sigma_{11,j}}^{old}, \quad D_{\sigma_{22,j}}^{new} = \beta D_{\sigma_{22,j}}^{old}, \quad D_{\sigma_{12,j}}^{new} = \beta D_{\sigma_{12,j}}^{old}. \quad (\text{B.11})$$

If $\beta=0$ the determinant is positive everywhere so that there is always an admissible value of β . If the determinant is not positive without correction, the highest $\beta \in [0,1]$ is chosen among the ones that satisfy the positivity of the determinant at each interface of the cell:

$$\Delta^* + \beta A \left(\pm \frac{\Delta x}{2} - \frac{\Delta x^2}{12} \frac{D_{\rho_j}}{\rho_j}\right) + \beta^2 B \left(\pm \frac{\Delta x}{2} - \frac{\Delta x^2}{12} \frac{D_{\rho_j}}{\rho_j}\right)^2 > 0. \quad (\text{B.12})$$

C Realizability of the MUSCL/HLL scheme

In [5] Berthon demonstrates the stability and the realizability of the MUSCL strategy for the Euler equations. Here we use the same ingredients to demonstrate the realizability of the MUSCL/HLL scheme proposed for the Anisotropic Gaussian model.

C.1 Realizability of the piecewise constant approximation

Proof of Theorem 3.1. Let us decompose a cell into three constant states: the left state M_L , the center state M_C and the right state M_R . Let us consider the following convex combination:

$$M_j = \alpha_1 M_L + \alpha_2 M_C + \alpha_3 M_R, \quad \text{with} \quad \alpha_1 + \alpha_2 + \alpha_3 = 1, \quad (\text{C.1})$$

where the parameters α_i represent the weights of each state into the total state M_j . Let us also consider that the border states M_L and M_R are evaluated at the cell interfaces using the reconstruction strategy so that, if the reconstruction strategy is realizable, the border states are realizable:

$$M_L = \tilde{M}_j(x_{j-1/2}), \quad M_R = \tilde{M}_j(x_{j+1/2}). \quad (\text{C.2})$$

To demonstrate the realizability of the piecewise constant approximation, we thus have to demonstrate that the M_C state is realizable. In the following we prove a sufficient condition for realizability. For the sake of simplicity we consider $\alpha_1 = \alpha_3$. For the density, we get:

$$\rho_C = \rho_j, \quad (\text{C.3})$$

so the positivity of the density is fulfilled for any value of α . For the velocities, we get:

$$u_c = \bar{u}_j + \frac{1-6\alpha_1}{1-2\alpha_1} \frac{D_\rho D_u}{\rho} \frac{\Delta x^2}{12}, \quad v_c = \bar{v}_j + \frac{1-6\alpha_1}{1-2\alpha_1} \frac{D_\rho D_v}{\rho} \frac{\Delta x^2}{12}. \quad (\text{C.4})$$

Finally for the covariance matrix, we get:

$$\sigma_C = \bar{\sigma} + \frac{D_\rho \mathbf{D}_\Sigma}{\rho_j} \frac{\Delta x^2}{12} \frac{1-6\alpha_1}{1-2\alpha_1} + \mathbf{D}_u^2 \frac{\Delta x^2}{12} \left(\frac{1-6\alpha_1}{1-2\alpha_1} + \frac{D_\rho^2}{\rho^2} \frac{\Delta x^2}{12} \frac{1}{1-2\alpha_1} \left(2 - \frac{(1-6\alpha_1)^2}{1-2\alpha_1} \right) \right). \quad (\text{C.5})$$

Then a sufficient condition to ensure the positivity of the central energies is $\alpha_1 = 1/6$:

$$\rho_j \sigma_{11,C} = \rho \bar{\sigma}_{11} + D_u^2 \frac{\Delta x^4}{48} \frac{D_\rho^2}{\rho} > 0, \quad \rho_j \sigma_{22,C} = \rho \bar{\sigma}_{22} + D_v^2 \frac{\Delta x^4}{48} \frac{D_\rho^2}{\rho} > 0. \quad (\text{C.6})$$

Moreover the positivity of the determinant must be imposed by an additional constraint on the velocity slopes:

$$\sigma_{11,C} \sigma_{22,C} - \sigma_{12,C}^2 = \bar{\sigma}_{11} \bar{\sigma}_{22} - \bar{\sigma}_{12}^2 + \frac{\Delta x^4}{48} \frac{D_\rho^2}{\rho^2} (\bar{\sigma}_{11} D_v^2 + \bar{\sigma}_{22} D_u^2 - 2\bar{\sigma}_{12} D_u D_v) > 0, \quad (\text{C.7})$$

$$H_R = -(\bar{\sigma}_{11} D_v^2 + \bar{\sigma}_{22} D_u^2 - 2\bar{\sigma}_{12} D_u D_v) < \frac{\bar{\sigma}_{11} \bar{\sigma}_{22} - \bar{\sigma}_{12}^2}{\frac{\Delta x^4}{48} \frac{D_\rho^2}{\rho^2}}. \quad (\text{C.8})$$

As for the slope limitation strategy, we thus introduce another parameter γ_R :

$$D_{u_j}^{new} = \gamma_R D_{u_j}^{old}, \quad D_{v_j}^{new} = \gamma_R D_{v_j}^{old}, \quad \gamma_R = \min \left(1, \sqrt{\frac{\bar{\sigma}_{11} \bar{\sigma}_{22} - \bar{\sigma}_{12}^2}{\frac{\Delta x^4}{48} \frac{D_\rho^2}{\rho^2} H_R}} \right). \quad (\text{C.9})$$

So we can always define the velocity slopes in such a way that the realizability of the center state M_C is verified, and which ends the proof. \square

C.2 Realizability of the HLL scheme

The HLL scheme is based on the definition of an intermediate state at each cell interface. The final solution is sought as a convex combination of each state on both sides of the interface and of the intermediate state. Then to prove the realizability of the HLL scheme, we have to prove the realizability of the intermediate state.

Proof of Theorem 3.2. Let us consider the intermediate state $\mathcal{M}_{j+1/2}^*$ defined in Eq. (3.8); it can be rewritten in the following manner:

$$\begin{aligned}\Delta\lambda_{j+1/2}\mathcal{M}_{j+1/2}^* &= \left(\mathcal{F}(\mathcal{M}_j) - \lambda_{\min}^j \mathcal{M}_j\right) + \left(\lambda_{\max}^{j+1} \mathcal{M}_{j+1} - \mathcal{F}(\mathcal{M}_{j+1})\right) \\ &= (u_j - \lambda_{\min}^j) \widetilde{\mathcal{M}}_j^* + (\lambda_{\max}^{j+1} - u_{j+1}) \widetilde{\mathcal{M}}_{j+1}^*,\end{aligned}\quad (\text{C.10})$$

where $\Delta\lambda_{j+1/2} = \lambda_{\max}^{j+1} - \lambda_{\min}^j > 0$, and where we have defined:

$$\widetilde{\mathcal{M}}_j^* = \left(\mathcal{F}(\mathcal{M}_j) - \lambda_{\min}^j \mathcal{M}_j\right) / (u_j - \lambda_{\min}^j), \quad (\text{C.11})$$

$$\widetilde{\mathcal{M}}_{j+1}^* = \left(\lambda_{\max}^{j+1} \mathcal{M}_{j+1} - \mathcal{F}(\mathcal{M}_{j+1})\right) / (\lambda_{\max}^{j+1} - u_{j+1}). \quad (\text{C.12})$$

Let us prove that $\widetilde{\mathcal{M}}_j^*$ is realizable, by developing its primitive variables. For the density, it naturally leads to $\widetilde{\rho}_j^* = \rho_j$. so that the density is positive since $\lambda_{\min}^j < u_j$. For the velocity no realizability constraint is necessary:

$$\widetilde{u}_j^* = \frac{\rho_j(u_j^2 + \sigma_{11,j}) - \rho_j u_j \lambda_{\min}^j}{\rho_j(u_j - \lambda_{\min}^j)} = u_j + \frac{\sigma_{11,j}}{u_j - \lambda_{\min}^j}, \quad (\text{C.13})$$

$$\widetilde{v}_j^* = \frac{\rho_j(u_j v_j + \sigma_{12,j}) - \rho_j v_j \lambda_{\min}^j}{\rho_j(u_j - \lambda_{\min}^j)} = v_j + \frac{\sigma_{12,j}}{u_j - \lambda_{\min}^j}. \quad (\text{C.14})$$

Finally positivity of the internal energies and the determinant of Σ is required:

$$\begin{aligned}\widetilde{\sigma}_{11,j}^* &= \frac{\rho_j(u_j^3 + 3u_j \sigma_{11,j}) - \rho_j(u_j^2 + \sigma_{11,j}) \lambda_{\min}^j}{\rho_j(u_j - \lambda_{\min}^j)} - (u_j^*)^2 \\ &= \sigma_{11,j} \left(1 - \frac{\sigma_{11,j}}{(u_j - \lambda_{\min}^j)^2}\right) > 0 \quad \text{if } \lambda_{\min}^j < u_j - \sqrt{\sigma_{11,j}},\end{aligned}\quad (\text{C.15})$$

$$\widetilde{\sigma}_{22,j}^* = \sigma_{22,j} \left(1 - \frac{\sigma_{11,j}}{(u_j - \lambda_{\min}^j)^2}\right) > 0 \quad \text{if } \lambda_{\min}^j < u_j - \sqrt{\sigma_{11,j}}, \quad (\text{C.16})$$

and

$$\widetilde{\sigma}_{11,j}^* \widetilde{\sigma}_{22,j}^* - (\widetilde{\sigma}_{12,j}^*)^2 = (\sigma_{11}\sigma_{22} - \sigma_{12}^2) \left(1 - \frac{\sigma_{11,j}}{(u_j - \lambda_{\min}^j)^2} \right) > 0 \quad \text{if } \lambda_{\min}^j < u_j - \sqrt{\sigma_{11,j}}. \quad (\text{C.17})$$

Repeating the same calculations for the state $\widetilde{\mathcal{M}}_{j+1}^*$, we get $\lambda_{\max}^{j+1} > u_{j+1} + \sqrt{\sigma_{11,j+1}}$ as a realizability constraint. Let us then define the two coefficients:

$$\widetilde{\beta}_j^* = \frac{u_j - \lambda_{\min}^j}{\Delta\lambda_{j+1/2}}, \quad \widetilde{\beta}_{j+1}^* = \frac{\lambda_{\max}^{j+1} - u_{j+1}}{\Delta\lambda_{j+1/2}}, \quad (\text{C.18})$$

then the convex combination

$$\widetilde{\mathcal{M}}_{j+1/2}^* = \frac{\widetilde{\beta}_j^*}{(\widetilde{\beta}_j^* + \widetilde{\beta}_{j+1}^*)} \widetilde{\mathcal{M}}_j^* + \frac{\widetilde{\beta}_{j+1}^*}{(\widetilde{\beta}_j^* + \widetilde{\beta}_{j+1}^*)} \widetilde{\mathcal{M}}_{j+1}^* \quad (\text{C.19})$$

is a realizable state. Thus, by the natural cone structure of the moment space, since $\mathcal{M}_{j+1/2}^* = (\widetilde{\beta}_j^* + \widetilde{\beta}_{j+1}^*) \widetilde{\mathcal{M}}_{j+1/2}^*$ and $\widetilde{\beta}_j^* + \widetilde{\beta}_{j+1}^* > 0$, we can conclude that $\mathcal{M}_{j+1/2}^*$ is realizable under the conditions $\lambda_{\min}^j < u_j - \sqrt{\sigma_{11,j}}$ and $\lambda_{\max}^{j+1} > u_{j+1} + \sqrt{\sigma_{11,j+1}}$ which ends the proof. \square

References

- [1] A. A. Amsden, P. J. O'Rourke, and T. D. Butler. Kiva II, a computer program for chemically reactive flows with sprays. Technical Report LA-11560-MS, Los Alamos National Laboratory, Los Alamos, New Mexico, 1989.
- [2] P. Andries, P. Le Tallec, J.-P. Perlat, and B. Perthame. The Gaussian-BGK model of Boltzmann equation with small Prandtl number. *Eur. J. of Mech. B - Fluids*, 19:813–830, 2000.
- [3] S. Balachandar and J.K. Eaton. Turbulent dispersed multiphase flow. *Annual Review of Fluid Mechanics*, 42:111–133, 2011.
- [4] C. Bardos, F. Golse, and D. Levermore. Fluid dynamic limits of kinetic equations. I. Formal derivations. *Journal of Statistical Physics*, 63, 1991.
- [5] C. Berthon. Stability of the MUSCL schemes for the Euler equations. *Commun. Math. Sci.*, 3(2):133–157, 2005.
- [6] C. Berthon. Numerical approximations of the 10-moment Gaussian closure. *Math. Comp.*, 75(256):1809–1831 (electronic), 2006.
- [7] P.L. Bhatnagar, E.P. Gross, and M. Krook. A model for collision proces in gases. I. Small amplitude processes in charged and neutral one-component systems. *Phys. Rev.*, 94:511–525, 1954.
- [8] G. A. Bird. *Molecular gas dynamics and the direct simulation of gas flows*. Oxford Science Publications, 42, 1994.
- [9] M. Boileau, C. Chalons, and M. Massot. Robust numerical coupling of pressure and pressureless gas dynamics equations for eulerian spray DNS and LES. *SIAM Journal of Scientific Computing*, submitted, pages 1–23, 2013. Available on HAL: <http://hal.archives-ouvertes.fr/hal-00906220>.

- [10] F. Bouchut. Nonlinear stability of finite volume methods for hyperbolic conservation laws and well-balanced schemes for sources. *Frontiers in Mathematics*. Birkhäuser Verlag, Basel, 2004.
- [11] F. Bouchut, S. Jin, and X. Li. Numerical approximations of pressureless and isothermal gas dynamics. *SIAM J. Num. Anal.*, 41:135–158, 2003.
- [12] S. L. Brown. Approximate Riemann solvers for moment models of dilute gases. PhD thesis, University of Michigan, 1996.
- [13] S. Brull and J. Schneider. On the ellipsoidal statistical model for polyatomic gases. *Cont. Mech. Thermodyn.*, 20:489–508, 2009.
- [14] C. Chalons, R. O. Fox, F. Laurent, M. Massot, and A. Vié. A multi-Gaussian quadrature-based moment method for dispersed multiphase flows. *SIAM Journal on Multiscale Modeling and Simulation*, submitted, 2013.
- [15] C. Chalons, R. O. Fox, and M. Massot. A multi-Gaussian quadrature method of moments for gas-particle flows in a LES framework. In *Proceedings of the Summer Program 2010, Center for Turbulence Research, Stanford University*, pages 347–358, Stanford, 2010.
- [16] C. Chalons, D. Kah, and M. Massot. Beyond pressureless gas dynamics: quadrature-based velocity moment models. *Communication in Mathematical Sciences*, 10(4):1241–1272, 2012.
- [17] C. Chalons, M. Massot, and A. Vié. An asymptotic preserving numerical scheme for the large eddy simulation of disperse phase flows. *SIAM Journal on Multiscale Modeling and Simulation*, submitted, 2014. available online at <http://hal.archives-ouvertes.fr/hal-00958108>.
- [18] O. Colin and M. Rudgyard. Development of high-order Taylor–Galerkin schemes for LES. *Journal of Computational Physics*, 162(2):338–371, 2000.
- [19] S. de Chaisemartin. Eulerian models and numerical simulation of turbulent dispersion for polydisperse evaporating sprays. PhD thesis, Ecole Centrale Paris, France, 2009. Available online at <http://tel.archives-ouvertes.fr/tel-00443982/en/>.
- [20] F. Doisneau. Eulerian modeling and simulation of polydisperse moderately dense coalescing spray flows with nanometric-to-inertial droplets: application to Solid Rocket Motors. PhD thesis, Ecole Centrale Paris, 2013. Available at <http://tel.archives-ouvertes.fr/tel-00966185>.
- [21] F. Doisneau, F. Laurent, A. Murrone, J. Dupays, and M. Massot. Eulerian multi-fluid models for the simulation of dynamics and coalescence of particles in solid propellant combustion. *J. Comput. Phys.*, 234:230–262, 2013.
- [22] F. Doisneau, O. Thomine, F. Laurent, A. Vié, J. Dupays, and M. Massot. Eulerian modeling and simulation of small scale trajectory crossing and coalescence for moderate-stokes-number spray flows. *Proceedings of the Summer Program 2012, Center for Turbulence Research, Stanford University*, pages 365–374, 2012.
- [23] J. Dombard. Direct Numerical Simulation of non-isothermal dilute sprays using the Mesoscopic Eulerian Formalism. PhD thesis, INP Toulouse, 2011.
- [24] G. Dufour. Modélisation multi-fluide eulérienne pour les écoulements diphasiques à inclusions dispersées. PhD thesis, Université Paul Sabatier Toulouse III, 2005.
- [25] J. K. Dukowicz. A particle-fluid numerical model for liquid sprays. *J. Comput. Phys.*, 35(2):229–253, 1980.
- [26] B. Einfeldt, C.D. Munz, P.L. Roe, and B. Sjögren. On Godunov-type Methods near low densities. *Journal of Computational Physics*, 92:273–295, 1991.
- [27] O. Emre, F. Laurent, S. de Chaisemartin, S. Jay, and M. Massot. Numerical analysis of a two-way coupled Eulerian high order moment method for the simulation of polydisperse evaporating sprays. *Journal of Computational Physics*, submitted, pages 1–28, 2013.
- [28] J. Ferry and S. Balachandar. A fast Eulerian method for disperse two-phase flow. *Int. J.*

- Multiphase Flow, 27:1199–1226, 2001.
- [29] P. Février, O. Simonin, and K. D. Squires. Partitioning of particle velocities in gas-solid turbulent flow into a continuous field and a spatially uncorrelated random distribution: theoretical formalism and numerical study. *J. Fluid Mech.*, 533:1–46, 2005.
 - [30] R.O. Fox. in “Computational Models for Turbulent Multiphase Reacting Flows”, Udine, July 2006,, chapter Fundamental of Polydisperse Multiphase Flows. CISM Courses and Lectures. Springer Verlag, 2007.
 - [31] V. Giovangigli and M. Massot. Asymptotic stability of equilibrium states for multicomponent reactive flows. *Math. Models Methods Appl. Sci.*, 8(2):251–297, 1998.
 - [32] F. Golse. The Boltzmann equation and its hydrodynamic limits. In *Evolutionary equations. Vol. II, Handb. Differ. Equ.*, pages 159–301. Elsevier/North-Holland, Amsterdam, 2005.
 - [33] H. Grad. *Principles of kinetic theory of gases, volume XII*. Springer-Verlag, 1958.
 - [34] B. Graille, T. Magin, and M. Massot. Kinetic theory of plasmas: Translational energy. *Mathematical Models and Methods in Applied Sciences*, 19:527–599, 2009.
 - [35] A. Harten, P.D. Lax, and B. van Leer. On upstream differencing and Godunov-type schemes for hyperbolic conservation laws. *SIAM Review*, 25(1):35–61, 1983.
 - [36] L.H. Holway Jr. New statistical models for kinetic theory: methods of construction. *The Physics of Fluids*, 9(9):1658–1673, 1966.
 - [37] J. J. Hylkema. Modélisation cinétique et simulation numérique d’un brouillard dense de gouttelettes. Application aux propulseurs à poudre. PhD thesis, Ecole Nat. Supérieure de l’Aéronautique et de l’Espace, 1999.
 - [38] D. Kah, F. Laurent, L. Fréret, S. de Chaisemartin, R. Fox, J. Reveillon, and M. Massot. Eulerian quadrature-based moment models for dilute polydisperse evaporating sprays. *Flow Turbulence and Combustion*, 85(3–4):649–676, 2010.
 - [39] D. Kah, F. Laurent, M. Massot, and S. Jay. A high order moment method simulating evaporation and advection of a polydisperse spray. *J. Comput. Phys.*, 231(2):394–422, 2012.
 - [40] A. Kaufmann, M. Moreau, O. Simonin, and J. Helie. Comparison between Lagrangian and mesoscopic Eulerian modelling approaches for inertial particles suspended in decaying isotropic turbulence. *J. Comput. Phys.*, 227:6448–6472, 2008.
 - [41] A. Larat, A. Vié, and M. Massot. A stable, robust and high order accurate numerical method for Eulerian simulation of spray and particle transport on unstructured meshes. *Annual Research Briefs of the CTR 2012, Center for Turbulence Research, Stanford University*, pages 205–216, 2012.
 - [42] F. Laurent and M. Massot. Multi-fluid modeling of laminar poly-dispersed spray flames: origin, assumptions and comparison of the sectional and sampling methods. *Combust. Theory and Modelling*, 5:537–572, 2001.
 - [43] F. Laurent, A. Vié, C. Chalons, R. O. Fox, and M. Massot. A hierarchy of Eulerian models for trajectory crossing in particle-laden turbulent flows over a wide range of Stokes numbers. *Annual Research Briefs of the CTR 2012, Center for Turbulence Research, Stanford University*, pages 193–204, 2012.
 - [44] R. J. LeVeque. *Finite volume methods for hyperbolic problems*. Cambridge Texts in Applied Mathematics. Cambridge University Press, Cambridge, 2002.
 - [45] C.D. Levermore. Moment closure hierarchies for kinetic theories. *J. Stat Phys.*, 83(5/6):1021–1065, 1996.
 - [46] C.D. Levermore and W.J. Morokoff. The Gaussian moment closure for gas dynamics. *SIAM J. Appl. Math.*, 59(1):72–96, 1998.
 - [47] C.D. Levermore, W.J. Morokoff, and B.T. Nadiga. Non-equilibrium partition function in the

- presence of heat flow. *Physics of Fluids*, 10:3214, 1998.
- [48] F.E. Marble. Dynamics of dusty gases. *Annual Review of Fluid Mechanics*, 2:397–446, 1970.
- [49] L. Martinez, A. Vié, S. Jay, A. Benkenida, and B. Cuenot. Large Eddy Simulation of Fuel sprays using the Eulerian Mesoscopic Approach. Validations in realistic engine conditions. In *ICLASS*, 2009.
- [50] E. Masi and Simonin. Algebraic-closure-based moment method for unsteady eulerian simulations of non-isothermal particle-laden turbulent flows at moderate stokes numbers in dilute regime. *Flow Turbulence and Combustion*, 92(1-2):121–145, 2014.
- [51] E. Masi, O. Simonin, E. Riber, P. Sierra, and L.Y.M. Gicquel. Development of an algebraic-closure-based moment method for unsteady eulerian simulations of particle-laden turbulent flows in very dilute regime. *International Journal of Multiphase Flow*, 58:257–278, 2014.
- [52] M. Massot. Eulerian multi-fluid models for polydisperse evaporating sprays, volume 492 of *CISM Courses and Lectures*, chapter in “Multiphase Reacting Flows: Modelling and Simulation”, Udine, July 2006, pages 79–123. Springer Wien New York (2007), 2007. D.L. Marchisio and R.O. Fox Editors.
- [53] M. Massot, R. Knikker, C. Péra, and J. Reveillon. Lagrangian/Eulerian analysis of the dispersion of evaporating droplets in a non-homogeneous turbulent flow. In *Proceedings of ICMF’04*, Yokohama, Japan, May 31 - June 3, 2004.
- [54] M. Massot, F. Laurent, D. Kah, and S. de Chaisemartin. A robust moment method for evaluation of the disappearance rate of evaporating sprays. *SIAM J. Appl. Math.*, 70(8):3203–3234, 2010.
- [55] J.G. Mc Donald and C.P.T. Groth. Towards realizable hyperbolic moment closures for viscous heat-conducting gas flows based on a maximum-entropy distribution. *Cont. Mech. Thermodyn.*, 25(5):573–603, 2012.
- [56] P. J. O’Rourke. Collective drop effects on vaporizing liquid sprays. PhD thesis, Los Alamos National Laboratory 87545, University of Princeton, 1981.
- [57] M.W. Reeks. On the dispersion of small particles suspended in an isotropic turbulent fluid. *J. Fluid Mech.*, 83(03):529–546, 1977.
- [58] A. Refloch, B. Courbet, A. Murrone, P. Villedieu, C. Laurent, P. Gilbank, J. Troyes, L. Tessé, G. Chaineray, J.B. Dargaud, E. Quémerais, and F. Vuillot. CEDRE software. Aerospace Lab, 2:1–10, 2011.
- [59] J. Reveillon and F.X. Demoulin. Effects of the preferential segregation of droplets on evaporation and turbulent mixing. *Journal of Fluid Mechanics*, 583:273–302, 2007.
- [60] E. Riber, M. Garcia, V. Moureau, H. Pitsch, O. Simonin, and T. Poinso. Evaluation of numerical strategies for les of two-phase reacting flows. *Proceedings of the Summer Program 2006*, Center for Turbulence Research, Stanford University, pages 197–213, 2006.
- [61] M. Sabat, A. Larat, A. Vié, and M Massot. Comparison of realizable schemes for the Eulerian simulation of disperse phase flows. *Proceedings of FVCA7*, accepted, Berlin, Germany, pages 1–8, 2014.
- [62] M. Sabat, A. Larat, A. Vié, and M Massot. On the development of high order realizable schemes for the Eulerian simulation of disperse phase flows on unstructured grids: a convex-state preserving Discontinuous Galerkin method. *Journal of Computational Physics*, submitted, 2014.
- [63] M. Sanjosé, J.-M. Senoner, F. Jaegle, B. Cuenot, S. Moreau, and T. Poinso. Fuel injection model for Euler-Euler and Euler-Lagrange large-eddy simulations of an evaporating spray inside an aeronautical combustor. *International Journal of Multiphase Flow*, 37(5):514–529, 2011.

- [64] P. Sierra. Modeling the dispersion and evaporation of sprays in aeronautical combustion chambers. PhD thesis, INP Toulouse, 2012.
- [65] R. M. C. So, L. H. Jin, and T. B. Gatski. An explicit algebraic Reynolds stress and heat flux model for incompressible turbulence: Part I Non-isothermal flow. *Theoretical and Computational Fluid Dynamics*, 17:351–376, 2004.
- [66] K. D. Squires and J.K. Eaton. Preferential concentration of particles by turbulence. *Physics of Fluids*, 3:1169–1178, 1991.
- [67] H. Struchtrup. *Macroscopic Transport Equations for Rarefied Gas Flows*. Springer, 2005.
- [68] E.F. Toro. *Riemann solvers and numerical methods for fluid dynamics*. Springer, 2009.
- [69] B. Van Leer. Toward the ultimate conservation difference scheme V. A second-order sequel to Godunov’s method. *J. Comput. Phys.*, 32(1):101–136, 1979.
- [70] F.-H. Vasilescu. Hamburger and Stieltjes moment problems in several variables. *Transactions of the American mathematical society*, 354(3):1265–1278, 2001.
- [71] A. Vié, C. Chalons, R. O. Fox, F. Laurent, and M. Massot. A multi-Gaussian quadrature method of moments for simulating high-Stokes-number turbulent two-phase flows. *Annual Research Briefs of the CTR 2011*, Center for Turbulence Research, Stanford University, pages 309–320, 2011.
- [72] A. Vié, S. Jay, B. Cuenot, and M. Massot. Accounting for Polydispersion in the Eulerian Large Eddy Simulation of an Aeronautical-type Configuration. *Flow Turbulence and Combustion*, 90(3):545–581, 2013.
- [73] A. Vié, F. Laurent, and M. Massot. A high order moment method for the simulation of polydisperse two-phase flows. *Comptes Rendus Mécanique*, 341(1–2):55–64, 2013.
- [74] A. Vié, F. Laurent, and M. Massot. Size-velocity correlations in hybrid high order moment/multi-fluid methods for polydisperse evaporating sprays: modeling and numerical issues. *Journal of Computational Physics*, 237:177–210, 2013.
- [75] A. Vié, E. Masi, O. Simonin, and M. Massot. On the direct numerical simulation of moderate-stokes-number turbulent particulate flows using Algebraic-Closure-Based and Kinetic-Based Moment Methods. In *Proceedings of the Summer Program 2012*, Center for Turbulence Research, Stanford University, pages 355–364, 2012.
- [76] F. A. Williams. Spray combustion and atomization. *Phys. Fluids*, 1:541–545, 1958.
- [77] F. A. Williams. *Combustion Theory (Combustion Science and Engineering Series)*. Ed. F. A. Williams (Reading, MA: Addison-Wesley), 1985.
- [78] C. Yuan and R.O. Fox. Conditional quadrature method of moments for kinetic equations. *J. Comput. Phys.*, 230(22):8216–8246, 2011.
- [79] L.I. Zaichik and V.M. Alipchenkov. Pair dispersion and preferential concentration of particles in isotropic turbulence. *Phys. Fluids*, 15:1776–1787, 2003.
- [80] L.I. Zaichik, V.M. Alipchenkov, and E.G. Sinaiski. *Particles in Turbulent Flows*. Wiley-VCH, Weinheim, Germany, 2008.
- [81] L.I. Zaichik, O. Simonin, and V.M. Alipchenkov. An Eulerian approach for large eddy simulation of particle transport in turbulent flows. *Journal of Turbulence*, 10(4):1–21, 2009.